potassium current that stabilizes excitability during the terminal phase of repolarization in the heart and the resting membrane potential in skeletal muscle.[11]

Approximately 40% patients with Andersen–Tawil syndrome do not harbor mutations in *KCNJ2*, suggesting the presence of other causative genes.[12] We identified a patient with periodic paralysis and characteristic ECG features suggestive of Andersen–Tawil syndrome but failed to find mutations in *KCNJ2*. Exome capture resequencing analysis revealed a novel mutation in *KCNJ5*. We investigated the functional consequences of the mutation using a heterologous expression system in *Xenopus* oocytes to understand its pathomechanism.

Figure 1 **Pedigree of the family and ECG recordings of the proband**

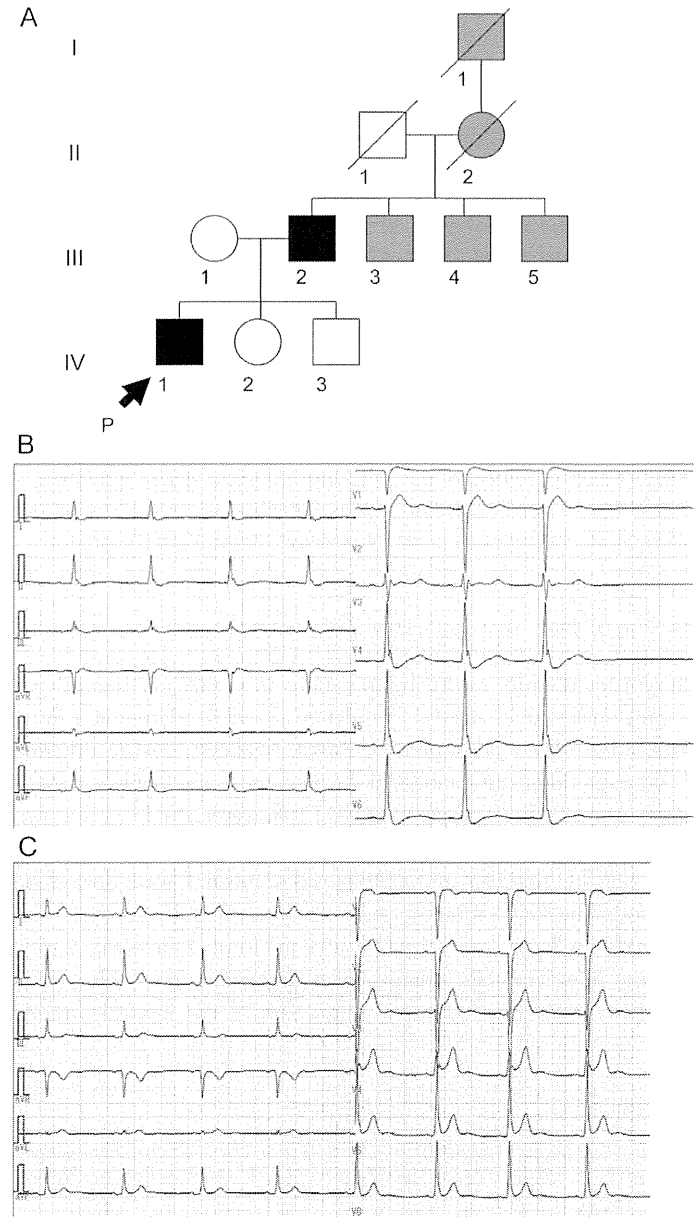

(A) Pedigree of the family. Filled symbols represent affected and empty symbols represent unaffected individuals. Gray symbols represent patients with arrhythmia lacking detailed information. DNA was available only from the proband. ECG recordings of the proband during the attack of hypokalemic periodic paralysis (B) and at the interictal state (C). In addition to prominent U waves, atrial standstill was also observed during the paralytic attack (B).

METHODS **Patient.** The proband (IV-1 in figure 1A) was a 35-year-old man who experienced periodic episodes of paralysis with reduced serum potassium concentrations starting at the age of 31 years. The episodes occurred several times in a year and lasted from 1 to 10 days. During a severe attack, the weakness, which initially manifested in the legs, extended to the upper limbs within several days and then gradually improved. The proband showed an abnormal decrement in the amplitude of compound motor action potentials in the prolonged exercise test at the interictal state. He showed no dysmorphic features, but had a family history of arrhythmia (figure 1A). The clinical data of other family members were not available because of lack of consent. His father (III-2) underwent pacemaker implantation because of bradycardia/tachycardia syndrome with atrial fibrillation. Three uncles, a grandmother, and a great-grandfather, all on his father's side, had arrhythmia; however, the details of their conditions were not available. Within the knowledge of the proband, no other family members had experience of paralytic attacks.

The proband had no cardiac symptoms, but the ECG recorded during the paralytic attack with a serum potassium concentration of 2.0 mEq/L exhibited prominent U waves and possible sinus arrest (figure 1B, right). The U waves were consistently observed at normal potassium concentration (figure 1C). His thyroid function was normal and he did not show hypertension or increased plasma aldosterone levels, which ruled out primary hyperaldosteronism.

Standard protocol approvals, registrations, and patient consents. We obtained informed consent from the patient using protocols approved by the Institutional Ethics Review Board of Osaka University.

Sanger sequencing. Genomic DNA was extracted from blood leukocytes. The regions encompassing known causative mutations for periodic paralysis in *SCN4A* and *CACNA1S* and the entire coding region of *KCNJ2* and *KCNJ18* were amplified using either Platinum Taq DNA Polymerase High Fidelity (Life Technologies, Carlsbad, CA) or the Advantage-GC2 PCR kit (Clontech, Mountain View, CA) (primer sequences are listed in table e-1 on the *Neurology*® Web site at Neurology.org).[13] The purified fragments were sequenced using an automated DNA sequencer (Big Dye Terminator version 3.1 and ABI3100; Life Technologies).

Exome capture resequencing analysis. We enriched exonic regions of genomic DNA using the SureSelect Human All Exon v.2 kit (Agilent Technologies, Santa Clara, CA), which covers 44 mega base pairs of the human genome or 98.2% of the CCDS (Consensus Coding Sequence) database and sequenced 50 base pairs of each tag in a single direction using the SOLiD 4 system (Life Technologies). We obtained 80.0×10^6 tags of 50–base pair reads and mapped 57.7×10^6 tags (72.1%) to the hg19/GRCh37 human genome, which yielded a mean coverage of 53.2 on the targeted exome regions. Next, we removed multiple-aligned reads,

© 2014 American Academy of Neurology. Unauthorized reproduction of this article is prohibited.

unreliable reads, and PCR duplicates using Avadis NGS 1.3 (Strand, San Francisco, CA). Single nucleotide variants (SNVs) and indels were called by Avadis NGS using default parameters. We restricted our analysis to 162 genes that encode ion channels and associated proteins (table e-2). We then excluded SNVs and indels that were registered in the nonclinical subset of dbSNP137, 1000 Genomes database, 6,500 genomes in the NHLBI ESP database (http://evs.gs.washington.edu/EVS/), or our cohort of 38 other diseases and controls. The other diseases in our cohort included congenital myasthenic syndromes, osteogenesis imperfecta, mitochondrial myopathies, and Schwartz–Jampel syndrome.

Immunoblotting. Skeletal muscle and heart tissues were taken at autopsy from control patients with disease (myotonic dystrophy type 1 and amyotrophic lateral sclerosis). Tissues were homogenized in a 10× volume of radioimmunoprecipitation assay buffer (25 mM Tris-HCl; pH 7.5; 150 mM NaCl; 1% NP-40; 1% sodium deoxycholate; and 0.1% sodium dodecyl sulfate) containing a protein inhibitor cocktail (Sigma-Aldrich, St. Louis, MO). The homogenate was centrifuged for 10 minutes at 10,000*g* and the supernatant was collected. Equal amounts of protein (20 μg) were separated by sodium dodecyl sulfate–polyacrylamide gel electrophoresis and transferred onto Immobilon-P membranes (Millipore, Bedford, MA), as previously described.[14] Blots were blocked for nonspecific protein binding with 5% (w/v) nonfat milk overnight and then incubated at room temperature for 1 hour with a 1:3,000-diluted antibody against Kir3.4 (AVIVA Systems Biology, Atlanta, GA) or GAPDH (glyceraldehyde 3-phosphate dehydrogenase) (Sigma-Aldrich). After repeated washings, the membranes were incubated at room temperature for 1 hour with peroxidase-conjugated goat anti-rabbit immunoglobulin G (1:30,000 dilution; GE Healthcare Biosciences, Pittsburgh, PA). The membranes were then washed, developed using an enhanced chemiluminescence kit (GE Healthcare Biosciences), and exposed to x-ray film.

Electrophysiology. Complementary RNAs (cRNAs) for mouse IRK1, which differs from human Kir2.1 by only 5 amino acids, and human Kir3.4 were expressed in *Xenopus* oocytes. Complementary DNAs cloned into the pGEMHE vector were kindly provided by Dr. Diomedes Logothetis (Virginia Commonwealth University). A site-directed mutagenesis kit (KOD-Plus Mutagenesis Kit; Toyobo, Osaka, Japan) was used to introduce the G387R mutation into the human Kir3.4 clone. The cRNAs were synthesized from linearized plasmid DNA using an mMESSAGE mMACHINE transcription kit (Life Technologies).

Xenopus oocytes were collected from frogs anesthetized in water containing 0.2% ethyl 3-aminobenzoate methanesulfonate salt (Sigma-Aldrich). The oocytes were isolated and defolliculated by treatment with type I collagenase (1.0 mg/mL; Sigma-Aldrich) and then injected with cRNAs that were quantified using a spectrophotometer (NanoDrop 2000; Thermo Fisher, Wilmington, DE). Injected oocytes were incubated for 2 to 3 days at 18°C in ND96 solution (5 mM HEPES; 96 mM NaCl; 2 mM KCl; 1.8 mM $CaCl_2$; and 1 mM $MgCl_2$; pH 7.5; supplemented with gentamicin and pyruvate).

Macroscopic currents were recorded with a 2-electrode voltage clamp using a bath-clamp amplifier (OC-725C; Harvard Apparatus, Holliston, MA). Stimulation, data acquisition, and data analysis were performed using the Patchmaster software (HEKA Elektronic, Lambrecht/Pfalz, Germany). Glass microelectrodes were filled with 3 M KCl, with a final resistance ranging from 0.2 to 1.0 MΩ. Recordings were performed at room temperature (22°C–25°C) in a bath solution containing 90 mM KCl, 3 mM $MgCl_2$, and 5 mM HEPES (pH 7.35–7.4). Step pulses ranging from −150 to +50 mV were applied from a holding potential of 0 mV for 200 milliseconds.

RESULTS Genome analyses of the proband. Genome samples from other members of the family were not available. Sanger nucleotide sequence analysis of the patient's DNA showed no causative mutations in *SCN4A* and *CACNA1S* (which were previously reported as being responsible for periodic paralysis) or in the entire coding region of *KCNJ2* and *KCNJ18*. Furthermore, an intragenic deletion or duplication in *KCNJ2* was excluded by the multiplex ligation-dependent probe amplification method (e-Methods and figure e-1).

The exome capture resequencing analysis yielded 44,550 SNVs and 1,852 indels. We restricted our analysis to 162 genes that encode ion channels and associated proteins (table e-2) and then excluded SNVs and indels registered in public single nucleotide polymorphism (SNP) databases (nonclinical subset of dbSNP137, 1000 Genomes database, and 6,500 genomes in the NHLBI ESP database) or our cohort of 38 other diseases and controls, which resulted in the identification of 3 heterozygous missense SNVs (table 1). Direct sequencing of the 3 SNVs by the Sanger method revealed that the SNVs in *RABGEF1* and *KCNT1* were artifacts, whereas the SNV in *KCNJ5*, G387R, was truly heterozygous in the patient. *KCNJ5* encodes a G-protein–activated inwardly rectifying potassium channel 4 (Kir3.4). Glycine at position 387 in the Kir3.4 is located at the C-terminus and is highly conserved across species, including mammals, chickens, and zebra fish. The G387R mutation was previously reported in a single Chinese family with LQT syndrome but absent in 528 controls.[15]

Table 1 **Heterozygous SNVs called by Avadis NGS in 162 genes encoding ion channels and associated proteins**

Chr.	Pos.	Gene	Ex.	SNVs	a.a.	Description	Variants/total[a]
chr7	66,270,306	*RABGEF1*	8	1,100 A/G	N334D[b]	RAB guanine nucleotide exchange factor (GEF) 1	8/54
chr9	138,656,938	*KCNT1*	12	1,097 A/G	H366R[b]	Potassium channel, subfamily T, member 1	6/26
chr11	128,786,525	*KCNJ5*	3	1,159 G/C	G387R	Potassium inwardly-rectifying channel, subfamily J, member 5	44/50

Abbreviations: a.a. = predicted amino acid substitution; Chr. = chromosome; Ex. = exon number; Pos. = position according to hg19/GRCh37; SNVs = single nucleotide variants.
[a] Number of variants and total reads after eliminating multiple-aligned reads, unreliable reads, and PCR duplicates.
[b] False SNV calls that were not detected by Sanger sequencing.

© 2014 American Academy of Neurology. Unauthorized reproduction of this article is prohibited.

Exome capture resequencing analysis covered the entire coding regions of *CACNA1S* 96.8-fold and *SCN4A* 54.4-fold on average. Two short segments of *SCN4A* were not covered by exome analysis and were directly sequenced by the Sanger method. These analyses detected a heterozygous synonymous G>A SNP, rs200175006, in *SCN4A*, which has a minor allelic frequency of 0.05% in normal population.

Immunoblotting. As mentioned above, the G387R mutation in the *KCNJ5* gene was previously identified in a family with LQT syndrome; however, no skeletal muscle features were described in that family.[15] The mutated Kir3.4 subunit has been reported to exert dominant-negative effects on Kir3.1/Kir3.4 channel complexes.[15] In the heart, Kir3.4 assembled with Kir3.1 forms an I_{KACh} current, which is predominantly expressed in the sinoatrial node and atria and contributes to the regulation of heart beat by acetylcholine; however, the function of G-protein–activated inwardly rectifying potassium channels in skeletal muscles has not been determined. Therefore, we investigated the existence and role of the Kir3.4 channel in skeletal muscle.

Figure 2 **Immunoblot of Kir3.4 in cardiac and skeletal muscle**

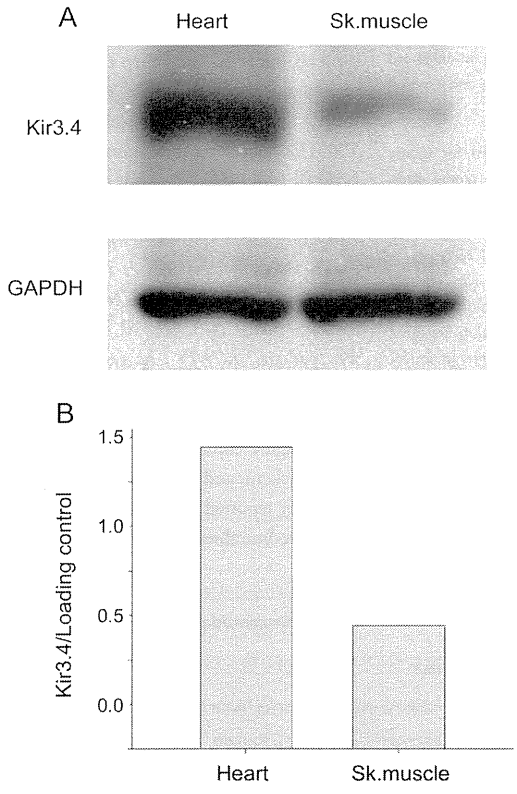

(A) Immunoblot analyses of the Kir3.4 subunit protein in the human heart and skeletal muscles are shown with loading control (GAPDH). (B) The densities of the Kir3.4 band were quantified and normalized to that of the loading control. GAPDH = glyceraldehyde 3-phosphate dehydrogenase; Sk. = skeletal.

Because messenger RNA for *KCNJ5* was detected in skeletal muscle tissue using an expression microarray assay, we tested whether the Kir3.4 protein is expressed in human skeletal muscles with immunoblotting, which revealed significant expression of the Kir3.4 protein in skeletal muscle from patients with myotonic dystrophy (figure 2) and amyotrophic lateral sclerosis (data not shown).

Electrophysiology. Although we found significant expression of Kir3.4 protein in human skeletal muscles, a significant G-protein–activated inwardly rectifying potassium current has never been physiologically recorded in mammalian skeletal muscles. Our patient exhibited clinical features that were indistinguishable from those of Andersen–Tawil syndrome, which is caused by loss-of-function mutations of *KCNJ2*; therefore, we suspected that mutated Kir3.4 may assemble heteromerically with Kir2.1, which is encoded by *KCNJ2*, thereby inhibiting inwardly rectifying potassium currents. Injection of Kir2.1 cRNA into oocytes induced a robust expression of strong inwardly rectifying potassium currents with a fast activation on hyperpolarization. Coinjection of Kir2.1 and Kir3.4 cRNAs did not change the properties of inward rectification (figure 3A). The coexpression of Kir2.1 with mutant Kir3.4 yielded a significant reduction in the inwardly rectifying potassium current compared with that observed for the coexpression of Kir2.1 with wild-type Kir3.4 (figure 3A). This reduction was observed at both conditions where cRNAs of Kir2.1 and Kir3.4 were injected with equal amounts and the amount of Kir2.1 cRNA was 10-fold greater than that of Kir3.4 (figure 3B). When wild-type or mutant Kir3.4 cRNA was injected without Kir2.1 cRNA, inwardly rectifying currents were observed; however, the amplitude of the currents was considerably smaller than that by Kir2.1 cRNA injection. These results suggest that the coexpression of mutant Kir3.4 subunits reduces inwardly rectifying potassium currents in the skeletal muscle, thus causing periodic paralysis.

***KCNJ5* gene analysis in a large cohort.** We performed Sanger sequencing analysis for mutations in *KCNJ5* in 3 Japanese cohorts of possible Andersen–Tawil syndrome, in which 46 families harbor *KCNJ2* mutations (see table e-1 for the primer sequences). Within 21 *KCNJ2*-negative cases, we identified a mutation of T158A (c.472A>G) in a single case, which originally showed prolonged QU on an ECG recorded at normal serum potassium concentration and later developed a hypokalemic paralytic attack and primary aldosteronism after 2 years.

DISCUSSION Using the exome capture resequencing analysis, we identified a *KCNJ5* mutation (which encodes the Kir3.4 subunit) in a patient with episodic

© 2014 American Academy of Neurology. Unauthorized reproduction of this article is prohibited.

Figure 3 **Electrophysiologic studies of the mutant Kir3.4 channel using *Xenopus* oocytes**

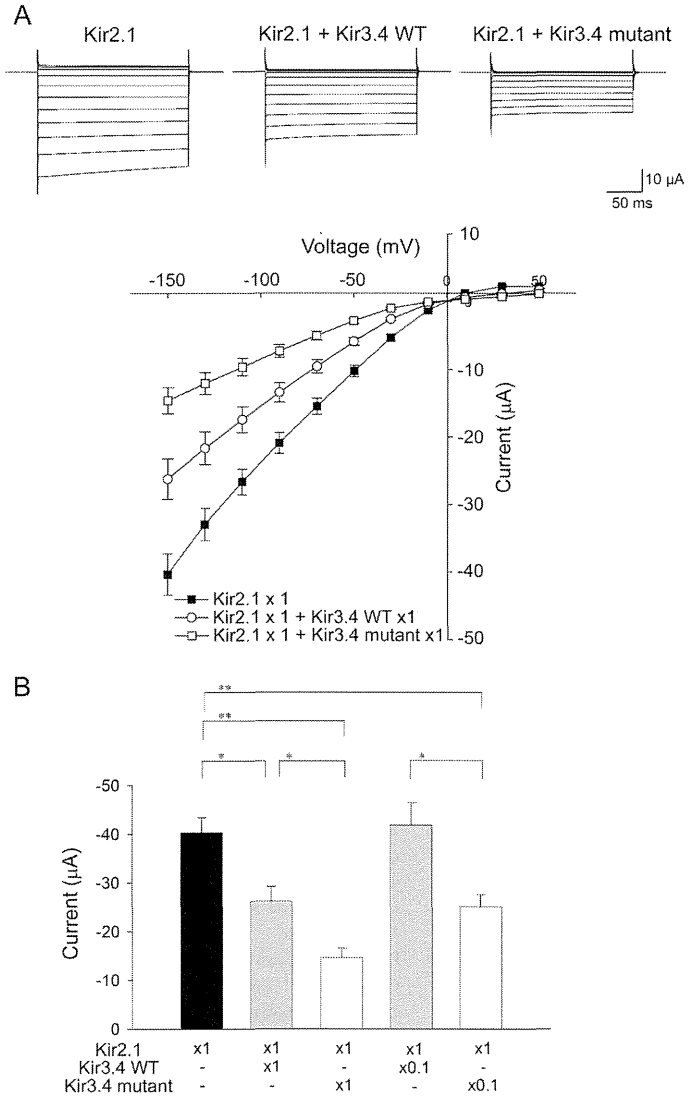

(A) Current-voltage relationships measured using step pulses for 200 milliseconds from −150 to +50 mV are shown. Symbols with error bars indicate the mean ± SEM (n = 20 for Kir2.1; 19 for Kir2.1 + Kir3.4 WT; 12 for Kir2.1 + Kir3.4 mutant). Representative current traces are shown at the top. The amount of complementary RNA (cRNA) injected into the oocytes was 3.4 ng per construct. (B) The currents induced by −150 mV step pulses are shown as a bar graph. Error bars indicate the mean ± SEM (n = 20, 19, 12, 21, and 15). The amount of cRNA for each construct was 3.4 ng for "×1" and 0.34 ng for "×0.1." *$p < 0.01$, **$p < 0.001$ (2-tailed unpaired *t* test). WT = wild type.

flaccid weakness and a characteristic TU-wave pattern, which are both suggestive of Andersen–Tawil syndrome. His family members presented autosomal-dominantly inherited arrhythmia, but apparent episodes of paralysis were observed only in the proband. The dysmorphic features did not appear to be present in any of the family members, including the proband. Although the syndrome was defined as a triad of potassium-sensitive periodic paralysis, ventricular dysrhythmias, and dysmorphic features, the paralytic attacks and dysmorphic features might not always be observed in Andersen–Tawil syndrome. It has been reported that the phenotypes are highly variable and the penetrance is not high in the *KCNJ2*-related Andersen–Tawil syndrome.[7]

It has been shown that Kir3.4 can form heteromeric channels with Kir2.1 when heterologously expressed in HEK293 cells or *Xenopus* oocytes.[16] There are no reports of the heteromerization of Kir3.4 with the Kir2.1 subunit in "native tissues"; however, Kir3.4 may have an effect on the inwardly rectifying potassium current. Reduction of the inwardly rectifying potassium current by the mutant Kir3.4 supports the notion that Kir3.4 modulates Kir2.1 and explains the clinical presentations in both skeletal and heart muscles in our case.

The G387R mutation of Kir3.4 was previously identified in a Chinese family presenting with LQT syndrome. In addition, the functional defect of the channel was characterized,[15] but the mechanism underlying the QT prolongation remained obscure. In the heart, it is known that the Kir3.4 subunit, mostly by heteromeric assembly with the Kir3.1 subunit, forms I_{KACh} channels, which are responsible for acetylcholine-dependent slowing of the heart rate. In fact, Kir3.4 knockout mice have an inability to regulate their heart rate in response to parasympathetic stimulation.[17,18] Therefore, it was initially unexpected that the decrease in I_{KACh}, which are predominantly expressed in atria, causes a defect in ventricular conductivity. The Kir2.1 subunit forms an inwardly rectifying potassium channel that provides repolarization during the most terminal phase of repolarization in ventricular cells. A suppression of inwardly rectifying potassium channels by the mutant Kir3.4 observed in *Xenopus* oocytes, if occurs in vivo, will cause a delay in the repolarization of ventricular cells and result in a prolonged QT (U) interval in ECG. Compared with other classic LQT syndromes, the prominent U wave is a hallmark of ECG findings in Andersen–Tawil syndrome caused by mutations of Kir2.1.[6,8] The similar U waves observed in our case may also support the alteration of inwardly rectifying potassium currents.

Despite the small density or absence of I_{KACh} current in skeletal muscles, we found significant expression of Kir3.4 protein in skeletal muscles. Because of the minimal role of I_{KACh} in skeletal muscle, it is unlikely that reduced I_{KACh} due to Kir3.4 mutation is responsible for the episodes of flaccid weakness. Coinjection of mutant Kir3.4 with the Kir2.1 subunit in *Xenopus* oocytes showed a reduction in the inwardly rectifying potassium current. The decrease in the inwardly rectifying potassium current caused by loss-of-function mutation in *KCNJ2* is the underlying mechanism of the episodic paralysis observed

© 2014 American Academy of Neurology. Unauthorized reproduction of this article is prohibited.

in Andersen–Tawil syndrome.[11] Although additional evidence is necessary, the Kir3.4 subunit in skeletal muscle may have a role in regulating the size of inwardly rectifying potassium currents.

It should be noted that germline and somatic mutations in *KCNJ5* have recently been reported to be responsible for familial hyperaldosteronism and aldosterone-producing adenomas, respectively.[19] Of interest, the other mutation of *KCNJ5* (T158A), which we identified in our cohort of possible Andersen–Tawil syndrome has previously been described as a germline mutation associated with familial hyperaldosteronism.[19] Although familial hyperaldosteronism is one of the causes of secondary hypokalemic periodic paralysis, it is unlikely that the clinical phenotypes of our cases are merely the consequences of hyperaldosteronism. Laboratory data in our case with the G387R mutation did not support the presence of hyperaldosteronism, and the TU complex in our case with the T158A mutation persisted at a normal concentration of serum potassium. Although further studies are required, some mutations of *KCNJ5* may show an overlapping phenotype with familial hyperaldosteronism and Andersen–Tawil syndrome.

In this study, we have identified a novel causative gene for Andersen–Tawil syndrome, *KCNJ5*, which encodes the Kir3.4 subunit, using an exome capture resequencing analysis. The mutant Kir3.4 subunit exerted an inhibitory effect on the inwardly rectifying potassium current, likely via heteromerization with Kir2.1. Although the heteromerization of Kir2.1 with the Kir3.4 subunit in native tissues should be further clarified, our case suggests that this mechanism has a role under both physiologic and pathologic conditions in skeletal muscle and the heart.

AUTHOR CONTRIBUTIONS

Dr. Yosuke Kokunai: designing experiments, acquisition of data. Dr. Tomohiko Nakata: acquisition of data. Dr. Mitsuru Furuta: acquisition of data, revising the manuscript. Dr. Souhei Sakata: designing experiments, acquisition of data. Dr. Hiromi Kimura, Dr. Takeshi Aiba, Dr. Masao Yoshinaga, and Dr. Yusuke Osaki: acquisition of data. Dr. Masayuki Nakamori: acquisition of data, drafting the manuscript. Dr. Hideki Itoh: analysis of data. Dr. Takako Sato: acquisition of data. Dr. Tomoya Kubota: drafting/revising the manuscript. Dr. Katsushige Kadota and Dr. Katsuro Shindo: acquisition of data. Dr. Hideki Mochizuki: revising the manuscript. Dr. Wataru Shimizu: acquisition of data. Dr. Minoru Horie: designing experiments, interpretation of data, and drafting/revising the manuscript. Dr. Yasushi Okamura: designing experiments, interpretation of data, and revising the manuscript. Dr. Kinji Ohno: designing experiments, interpretation of data, and drafting/revising the manuscript. Dr. Masanori P. Takahashi: study concept or design, designing experiments, interpretation of data, and drafting/revising the manuscript.

ACKNOWLEDGMENT

The authors thank Dr. Diomedes Logothetis for kindly providing the IRK1 and Kir3.4 plasmids, Drs. Hisako Katayama and Takekazu Ohi for referring the patient, and Ms. Kimie Hayashi for her technical assistance.

STUDY FUNDING

Supported by research grants from the Ministry of Health, Labour and Welfare, Intramural research grant (23-5) of the National Center of Neurology and Psychiatry, and grants-in-aid from the Japan Society for the Promotion of Science (to K.O. and M.P.T.).

DISCLOSURE

Y. Kokunai, T. Nakata, M. Furuta, S. Sakata, H. Kimura, T. Aiba, M. Yoshinaga, Y. Osaki, M. Nakamori, H. Itoh, T. Sato, T. Kubota, K. Kadota, K. Shindo, H. Mochizuki, W. Shimizu, M. Horie, and Y. Okamura report no disclosures relevant to the manuscript. K. Ohno and M. Takahashi received funding from the Ministry of Health, Labour and Welfare of Japan, National Center of Neurology and Psychiatry, and Japan Society for the Promotion of Science. Go to Neurology.org for full disclosures.

Received June 9, 2013. Accepted in final form December 16, 2013.

REFERENCES

1. Raja Rayan DL, Hanna MG. Skeletal muscle channelopathies: nondystrophic myotonias and periodic paralysis. Curr Opin Neurol 2010;23:466–476.
2. Venance SL, Cannon SC, Fialho D, et al. The primary periodic paralyses: diagnosis, pathogenesis and treatment. Brain 2006;129:8–17.
3. Jurkat-Rott K, Lehmann-Horn F. Paroxysmal muscle weakness: the familial periodic paralyses. J Neurol 2006; 253:1391–1398.
4. Tawil R, Ptacek LJ, Pavlakis SG, et al. Andersen's syndrome: potassium-sensitive periodic paralysis, ventricular ectopy, and dysmorphic features. Ann Neurol 1994;35: 326–330.
5. Andersen ED, Krasilnikoff PA, Overvad H. Intermittent muscular weakness, extrasystoles, and multiple developmental anomalies: a new syndrome? Acta Paediatr Scand 1971;60:559–564.
6. Tristani-Firouzi M, Jensen JL, Donaldson MR, et al. Functional and clinical characterization of KCNJ2 mutations associated with LQT7 (Andersen syndrome). J Clin Invest 2002;110:381–388.
7. Kimura H, Zhou J, Kawamura M, et al. Phenotype variability in patients carrying KCNJ2 mutations. Circ Cardiovasc Genet 2012;5:344–353.
8. Zhang L, Benson DW, Tristani-Firouzi M, et al. Electrocardiographic features in Andersen-Tawil syndrome patients with KCNJ2 mutations: characteristic T-U-wave patterns predict the KCNJ2 genotype. Circulation 2005; 111:2720–2726.
9. Plaster NM, Tawil R, Tristani-Firouzi M, et al. Mutations in Kir2.1 cause the developmental and episodic electrical phenotypes of Andersen's syndrome. Cell 2001;105:511–519.
10. Zobel C, Cho HC, Nguyen TT, et al. Molecular dissection of the inward rectifier potassium current (IK1) in rabbit cardiomyocytes: evidence for heteromeric co-assembly of Kir2.1 and Kir2.2. J Physiol 2003;550:365–372.
11. Tristani-Firouzi M, Etheridge SP. Kir 2.1 channelopathies: the Andersen-Tawil syndrome. Pflugers Arch 2010;460: 289–294.
12. Donaldson MR, Yoon G, Fu YH, Ptacek LJ. Andersen-Tawil syndrome: a model of clinical variability, pleiotropy, and genetic heterogeneity. Ann Med 2004;36(suppl 1): 92–97.
13. Ryan DP, da Silva MR, Soong TW, et al. Mutations in potassium channel Kir2.6 cause susceptibility to thyrotoxic hypokalemic periodic paralysis. Cell 2010;140:88–98.
14. Nakamori M, Kimura T, Fujimura H, Takahashi MP, Sakoda S. Altered mRNA splicing of dystrophin in type 1 myotonic dystrophy. Muscle Nerve 2007;36:251–257.
15. Yang Y, Liang B, Liu J, et al. Identification of a Kir3.4 mutation in congenital long QT syndrome. Am J Hum Genet 2010;86:872–880.

© 2014 American Academy of Neurology. Unauthorized reproduction of this article is prohibited.

16. Ishihara K, Yamamoto T, Kubo Y. Heteromeric assembly of inward rectifier channel subunit Kir2.1 with Kir3.1 and with Kir3.4. Biochem Biophys Res Commun 2009;380:832–837.
17. Wickman K, Nemec J, Gendler SJ, Clapham DE. Abnormal heart rate regulation in GIRK4 knockout mice. Neuron 1998;20:103–114.
18. Kovoor P, Wickman K, Maguire CT, et al. Evaluation of the role of I(KACh) in atrial fibrillation using a mouse knockout model. J Am Coll Cardiol 2001;37:2136–2143.
19. Choi M, Scholl UI, Yue P, et al. K+ channel mutations in adrenal aldosterone-producing adenomas and hereditary hypertension. Science 2011;331:768–772.

Mitigate Opioid Misuse in Your Practice

100 people die from drug overdoses every day in the United States.* Learn how to mitigate opioid misuse in your practice with the AAN's newest NeuroPI™ performance improvement module on Chronic Opioid Therapy.

- Helps address both the Performance in Practice (PIP) and Continuing Medical Education (CME) components of Maintenance of Certification (MOC), as mandated by the American Board of Psychiatry and Neurology (ABPN)
- Tackles the timely issue of chronic opioid therapy for non-cancer pain
- Offers measures to address strategies for mitigating opioid misuse
- Features educational resources, links to clinical tools, and patient education materials

Visit *www.aan.com/view/neuropi* today!

**CDC. Vital Signs: Overdoses of Prescription Opioid Pain Relievers–United States, 1999–2008. MMWR 2011;60:1–6*

Earn 20 CME Credits Toward MOC with New NeuroPI℠ Modules

Choose from the latest lineup of quality modules to join the AAN's exclusive performance improvement programs designed to help you address both the Performance in Practice (PIP) and Continuing Medical Education (CME) components of Maintenance of Certification (MOC).

- ***NEW!* Distal Symmetric Polyneuropathy (DSP)** includes **eight quality measures**, addressing accurate and appropriate evaluation/monitoring of DSP and associated symptoms to guide treatment options, patient safety, and best practices to assist patients in managing their pain and improving quality of life
- **Acute Stroke** addresses **six quality measures**, including deep vein thrombosis prophylaxis (DVT) for ischemic stroke or intracranial hemorrhage, discharged on antiplatelet therapy, dysphagia screening, rehabilitation service considerations, and more
- **Dementia** includes **10 quality measures** addressing underuse of effective services and patient-centered care strategies, and patient safety issues

Learn about all of the other available modules and purchase yours today:
www.aan.com/view/neuropi

© 2014 American Academy of Neurology. Unauthorized reproduction of this article is prohibited.

Journal of the American College of Cardiology
© 2014 by the American College of Cardiology Foundation
Published by Elsevier Inc.

Vol. 63, No. 8, 2014
ISSN 0735-1097/$36.00
http://dx.doi.org/10.1016/j.jacc.2013.08.1648

PRE-CLINICAL RESEARCH

A Molecular Mechanism for Adrenergic-Induced Long QT Syndrome

Jie Wu, PhD,*†‡ Nobu Naiki, MD,† Wei-Guang Ding, MD, PhD,‡ Seiko Ohno, MD, PhD,† Koichi Kato, MD,† Wei-Jin Zang, PhD,* Brian P. Delisle, PhD,§ Hiroshi Matsuura, MD, PhD,‡ Minoru Horie, MD, PhD†

Xi'an, China; Otsu, Japan; and Lexington, Kentucky

Objectives This study sought to explore molecular mechanisms underlying the adrenergic-induced QT prolongation associated with *KCNQ1* mutations.

Background The most frequent type of congenital long QT syndrome is LQT1, which is caused by mutations in the gene (*KCNQ1*) that encodes the alpha subunit of the slow component of delayed rectifier K^+ current (I_{Ks}) channel. We identified 11 patients from 4 unrelated families that are heterozygous for *KCNQ1*-G269S. Most patients remained asymptomatic, and their resting corrected QT intervals ranged from normal to borderline but were prolonged significantly during exercise.

Methods Wild-type (WT) *KCNQ1* and/or *KCNQ1*-G269S (G269S) were expressed in mammalian cells with *KCNE1*. I_{Ks}-like currents were measured in control conditions or after isoproterenol or protein kinase A (PKA) stimulation using the patch-clamp technique. Additionally, experiments that incorporated the phosphomimetic *KCNQ1* substitution, S27D, in WT or *KCNQ1*-G269S were also performed.

Results The coexpression of WT-*KCNQ1* with varying amounts of G269S decreased I_{Ks}, shifted the current-voltage *I-V* relation of I_{Ks} to more positive potentials, and accelerated the I_{Ks} deactivation rates in a concentration-dependent manner. In addition, the coexpression of G269S and WT blunted the activation of I_{Ks} in response to isoproterenol or PKA stimulation. Lastly, a phosphomimetic substitution in G269S did not show an increased I_{Ks}.

Conclusions G269S modestly affected I_{Ks} in control conditions, but it almost completely blunted I_{Ks} responsiveness in conditions that simulate or mimic PKA phosphorylation of *KCNQ1*. This insensitivity to PKA stimulation may explain why patients with G269S mutation showed an excessive prolongation of QT intervals on exercise. (J Am Coll Cardiol 2014;63:819–27) © 2014 by the American College of Cardiology Foundation

Congenital long QT syndrome (LQTS) is characterized by an abnormal QT interval prolongation on the electrocardiogram (ECG), syncope due to a polymorphic ventricular tachycardia called "torsade de pointes," and ventricular fibrillation (1,2). At least 13 genes are responsible for different subtypes of the syndrome (LQT1 to LQT13), with LQT1 being the most common and accounting for approximately 40% to 50% of genotyped patients (3,4). LQT1 is caused by mutations in *KCNQ1*, the alpha subunit of the slow component of delayed rectifier K^+ current (I_{Ks}), which is a major repolarizing current during the plateau phase of cardiac action potentials (5).

See page 828

The impaired expression or dysfunction of I_{Ks} channels (6,7) can lead to a prolongation in the cardiac action potential and the QT interval on an ECG (7,8). A major role for I_{Ks} is to maintain the ventricular action potential duration by offsetting the increase in L-type Ca^{2+} current ($I_{Ca,L}$) after adrenergic stimulation. Adrenergic stimulation activates protein kinase A (PKA), which directly increases I_{Ks} by phosphorylating the *KCNQ1* alpha subunit at S27 (8). Not surprisingly, most

From the *Department of Pharmacology, Medical School of Xi'an Jiaotong University, Xi'an, China; †Department of Cardiovascular and Respiratory Medicine, Shiga University of Medical Science, Otsu, Japan; ‡Department of Physiology, Shiga University of Medical Science, Otsu, Japan; and the §Department of Physiology, University of Kentucky, Lexington, Kentucky. This work was supported by research grants from the Ministry of Education, Culture, Science, and Technology of Japan (to Dr. Horie); Health Science Research Grants from the Ministry of Health, Labor and Welfare of Japan for Clinical Research on Measures for Intractable Diseases (to Dr. Horie); Translational Research Funds from Japan Circulation Society (to Dr. Horie); and National Natural Science Foundation of China (#81273501 to Drs. Wu and Ding). All other authors have reported that they have no relationships relevant to the contents of this paper to disclose. Drs. Wu and Naiki contributed equally to this paper.

Manuscript received June 16, 2013; revised manuscript received August 5, 2013, accepted August 26, 2013.

Abbreviations and Acronyms

cDNA = complementary deoxyribonucleic acid
CHO = Chinese hamster ovary
DNA = deoxyribonucleic acid
ECG = electrocardiogram
FK = forskolin
HEK293 = human embryonic kidney 293
IBMX = 3-isobutyl-l-methyl-xanthine
$I_{Ca,L}$ = L-type Ca^{2+} current
I_{Ks} = the slow component of delayed rectifier K^+ current
I-V = current-voltage
LQTS = long QT syndrome
QTc = corrected QT
PBS = phosphate-buffered saline
PKA = protein kinase A
WT = wild type

LQT1 patients experience triggered cardiac events during adrenergic stimulation (i.e., while exercising) (9,10).

More recently, we identified a heterozygous missense *KCNQ1* mutation, G269S, in 11 patients from 4 unrelated families. Similar to previous clinical reports (10–12), most of our patients have normal to borderline corrected QT (QTc) intervals at rest, but their QTc intervals are significantly prolonged after exercise. We characterize the functional consequences of the I_{Ks} channel reconstituted with G269S in mammalian cells and provide important insight into molecular mechanisms underlying the adrenergic-induced LQTS. Specifically, we found G269S modestly affected I_{Ks} but severely blunted the increase in I_{Ks} with isoproterenol, pharmacological activators of PKA, and with the PKA phosphomimetic mutation *KCNQ1*-S27D. These findings may explain why patients with G269S mutation showed an excessive prolongation of QT intervals on exercise and suggest a potential benefit of beta-blocker therapy.

Methods

Clinical investigation and genetic testing. The clinical diagnosis of LQTS was referred to the criteria of Schwartz et al. (2). The protocol for genetic analysis was approved by the institutional ethics committee and performed under its guidelines. Written informed consent was obtained from every subject before the analysis. Genomic deoxyribonucleic acid (DNA) used for genetic evaluation was isolated from venous blood lymphocytes. In addition to *KCNQ1*, genetic screening for mutations in other LQTS-related genes including *SCN5A*, *KCNH2*, *KCNE1*, *KCNE2*, and *KCNJ2* was conducted by denaturing high-performance liquid chromatography (WAVE system, Transgenomic Inc., Omaha, Nebraska). For abnormal screening patterns, sequencing was performed with an automated sequencer (ABI PRISM 3100x, Applied Biosystems, Foster City, California).

Heterologous expression of cDNA in CHO and HEK293 cells. Full-length complementary deoxyribonucleic acid (cDNA) encoding human wild-type (WT) *KCNQ1* (GenBank AF000571, Institut de Pharmacologie Moleculaire et Cellulaire, CNRS, Valbonne, France) was subcloned into a pIRES2-EGFP expression vector. *KCNQ1*-G269S, *KCNQ1*-S27D, and *KCNQ1*-(S27D-G269S) mutants were constructed using a Quick Change II XL site-directed mutagenesis kit (Stratagene, La Jolla, California), and they were also subcloned into the pIRES2-EGFP expression vector. Full-length cDNA encoding human *KCNE1* (GenBank M26685) subcloned into the pCDNA3.1 expression vector was obtained by polymerase chain reaction from human heart cDNA library (Clontech, Mountain View, California). Full-length cDNA encoding human A-kinase-anchoring protein 9 (Yotiao or AKAP9) was subcloned into pCDNA3.1 expression vector (Department of Bio-Informational Pharmacology, Tokyo Medical and Dental University, Japan). *KCNQ1*-WT and/or its mutants, *KCNE1* and Yotiao cDNA were transiently transfected into Chinese hamster ovary (CHO) or human embryonic kidney 293 (HEK293) cells using Lipofectamine (Invitrogen Life Technologies Inc., Carlsbad, California) according to the manufacturer's instructions.

Solutions and chemicals. The pipette solution contained (in mmol/l) 70 potassium aspartate, 40 KCl, 10 KH_2PO_4, 1 $MgSO_4$, 3 Na_2 adenosine triphosphate (Sigma, St. Louis, Missouri), 0.1 Li_2 Guanosine-5'-triphosphate (Roche Diagnostics GmbH, Mannheim, Germany), 5 ethylene glycol tetraacetic acid, and 5 *N*-2-hydroxyethylpiperazine-*N*-2-ethanesulfonic acid; and the pH was adjusted to 7.2 with KOH. The extracellular solution contained (in mmol/l) 140 NaCl, 5.4 KCl, 1.8 $CaCl_2$, 0.5 $MgCl_2$, 0.33 NaH_2PO_4, 5.5 glucose, and 5.0 *N*-2-hydroxyethylpiperazine-*N*-2-ethanesulfonic acid; the pH was adjusted to 7.4 with NaOH. Isoproterenol (Sigma) was dissolved in distilled water (containing 1 mmol/l ascorbic acid) to yield 10 mmol/l stock solution and kept in the dark at 4°C. Forskolin (FK, Sigma) and 3-isobutyl-l-methyl-xanthine (IBMX, Sigma) were respectively dissolved in dimethyl sulfoxide (Sigma) to yield stock solutions of 5 mmol/l and 15 mmol/l, respectively.

Electrophysiological recordings and data analysis. Forty-eight hours after transfection, cells attached to a glass coverslip were transferred to a 0.5-ml bath chamber perfused with extracellular solution and maintained at 25°C. Patch-clamp experiments were conducted on green fluorescent protein-positive cells. Whole-cell membrane currents were recorded with an EPC-8 patch-clamp amplifier (HEKA, Lambrecht, Germany). I_{Ks} were evoked by depolarizing voltage-clamp steps given from a holding potential of −80 mV to various test potentials. I_{Ks} amplitude was determined by measuring the amplitude of tail current elicited on repolarization to −50 mV following 2-s depolarization to 30 mV every 10 s, and currents were normalized to the cell membrane capacitance to obtain current densities (pA/pF). Voltage-dependence of I_{Ks} activation was evaluated by fitting the *I-V* relation of the tail currents to a Boltzmann equation: $I_{K,tail} = 1/[1+\exp([V_h - V_m]/k)]$, where $I_{K,tail}$ is the tail current amplitude density, V_h is the voltage at half-maximal activation, V_m is the test potential, and k is the slope factor. The deactivation kinetics of I_{Ks} after depolarization was determined by a single exponential fit of tail current trace.

Immunocytochemistry. Forty-eight hours after transfection, CHO cells were fixed with 3.7% formaldehyde in

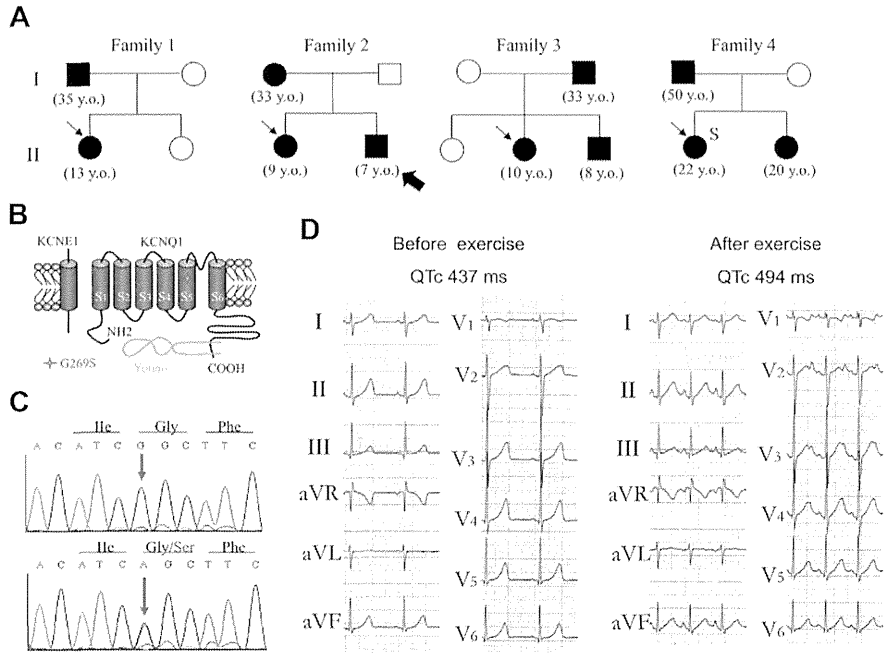

Figure 1 **Molecular Discovery and Clinical Characterization of *KCNQ1*-G269S**

(A) Four pedigrees of patients carrying the G269S mutation. **Solid symbols** indicate mutation carriers, arrows probands, and symptomatic patient (S). **Square and circle symbols** represent male and female subjects. **(B)** Predicted topology of I_{Ks} channel. **Red asterisk** indicates the location of G269S mutation. **(C)** A representative result of deoxyribonucleic acid sequence analysis: upper trace, control and lower, the proband in Family #2. **Red arrows** indicate the location of heterozygous mutation. **(D)** Twelve-lead electrocardiograms (left: resting and right: after exercise) in a 7-year-old (y.o.) boy from Family #2 **(bold arrow)**. QTc = corrected QT interval.

phosphate-buffered saline (PBS) for 10 min at room temperature, rinsed once in PBS, and permeabilized with 0.2% triton X-100 in PBS. Cells were blocked with 5% bovine serum albumin in PBS for 30 min and then incubated overnight at 4°C with anti-Kv7.1 (*KCNQ1*, Santa Cruz Biotechnology, Inc., Santa Cruz, California) antibody against its C-terminus at 1:2,000 dilution. Following incubation, cells were labeled with AlexaFluor 488-conjugated goat antirabbit immunoglobulin G (Molecular Probes, Eugene, Oregon) at 1:500 dilution. Immunofluorescence stained cells were captured using a confocal laser scanning microscope (LSM META 510, Carl Zeiss, Berlin, Germany).

All data are expressed as mean ± SE (QTc as mean ± SD), with the number of experiments in parentheses. Statistical comparisons were analyzed using unpaired Student *t* test and 1-way or 2-way analysis of variance with Newman-Keuls post hoc test. A p value of <0.05 was considered statistically significant.

Results

Case description. Genotype analyses of 551 consecutive LQTS probands identified 4 unrelated carriers with the *KCNQ1*-G269S mutation. Figure 1A shows 4 family pedigrees for the different probands (arrows). Figure 1B shows the location of the mutation (transmembrane domain S5) in the *KCNQ1* alpha subunit, and the lower panel in Figure 1C shows representative results of a genotype-positive patient's sequencing data (805G>A).

Figure 1D depicts 2 sets of 12-lead ECG recorded from a 7-year-old boy in Family #2 (Fig. 1A, bold arrow). His resting QTc interval was 437 ms, but it was prolonged to 494 ms after exercise. The boy was asymptomatic, but his maternal grandfather died suddenly at the age of 28 years (the detailed clinical information is not available). In Family #4, the 22-year-old female proband experienced sudden syncope, which recovered soon and was suspected to be due to ventricular tachyarrhythmia, while dancing, but her symptoms have disappeared after receiving beta-adrenergic blocker metoprolol tartrate for 42 months.

We performed an exercise tolerance test in 8 of the 11 mutation carriers (Fig. 1A). The mean resting QTc intervals were 441.6 ± 44.5 ms but significantly ($p < 0.05$) prolonged to 485.5 ± 14.4 ms after exercise. Therefore, *KCNQ1*-G269S might minimally affect I_{Ks} at rest but impair the up-regulation of I_{Ks} by PKA, because the exercise stress (PKA activation) does not prolong the QTc interval in control subjects (13).

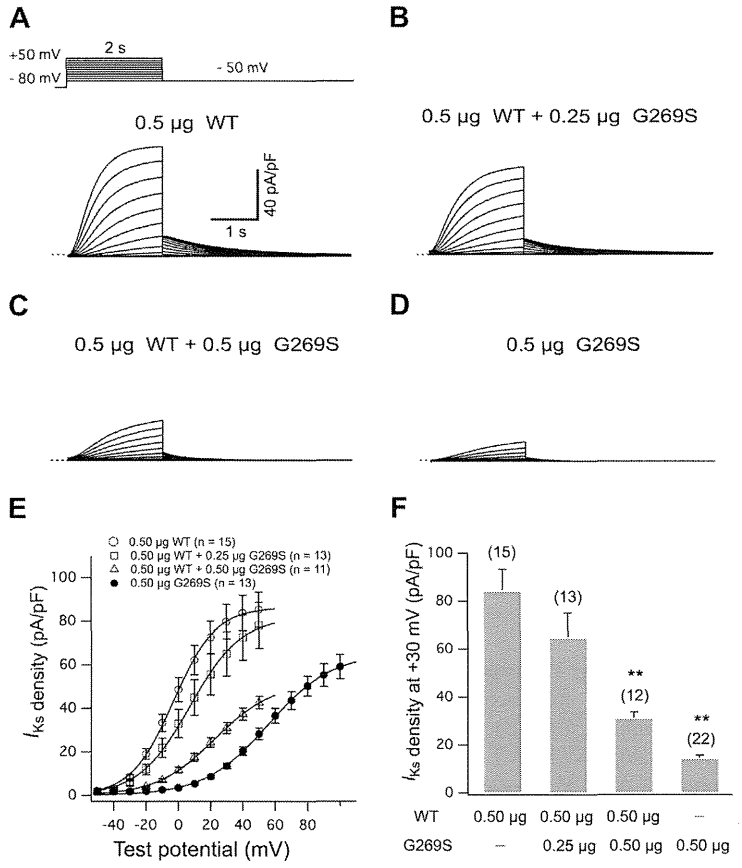

Figure 2 **G269S Decreases I_{Ks} in a Mutant Concentration-Dependent Manner**

Representative current traces recorded from Chinese hamster ovary cells expressing 0.5 μg *KCNE1* with 0.5 μg *KCNQ1*-WT **(A)**, 0.5 μg *KCNQ1*-WT + 0.25 μg *KCNQ1*-G269S **(B)**, 0.5 μg *KCNQ1*-WT + 0.5 μg *KCNQ1*-G269S **(C)**, and 0.5 μg *KCNQ1*-G269S **(D)**. The slow component of delayed rectifier K^+ current (I_{Ks}) was activated by depolarizing voltage-clamp steps **(inset in A)** given from a holding potential of −80 mV to potentials between −50 and +50 mV in 10-mV increments for 2 s. **Dashed line** indicates zero current level. **(E)** Current-voltage (*I-V*) relations for tail I_{Ks} elicited after the voltage-step to −50 mV from various test potentials. **(F)** Bar graphs showing the mean peak tail I_{Ks} densities recorded on repolarization to −50 mV following 2-s depolarization to 30 mV for the different transfection conditions. **p < 0.01 versus *KCNQ1*-WT. WT = wild type.

***KCNQ1*-G269S mutation causes a mild loss-of-function in I_{Ks} in control conditions.** Figures 2A to 2D show 4 sets of representative current traces recorded from CHO cells expressing *KCNE1* with *KCNQ1*-WT, *KCNQ1*-WT + *KCNQ1*-G269S, and *KCNQ1*-G269S, respectively. Cells transfected with varying amounts of G269S cDNA reduced both the steady state and tail I_{Ks} amplitudes in a concentration-dependent manner.

Figure 2E shows the current-voltage (*I-V*) relations for tail I_{Ks} elicited after the voltage-step to −50 mV from various test potentials, and Figure 2F summarizes tail I_{Ks} densities under 4 different conditions. Compared with WT, G269S alone or WT + G269S significantly decreased the mean I_{Ks} density for voltages between −20 mV and 50 mV and the mutation displayed a moderate dominant-negative suppression on WT-*KCNQ1* function.

Figure 3A shows the normalized *I-V* relations for tail I_{Ks} in Figure 2E. The individual *I-V* relations were described by the Boltzmann equation to calculate the voltage for half-maximal activation (V_h) and slope factor (k) values (Table 1). Coexpressing WT with different amounts of G269S increased the V_h and k in a concentration-dependent manner.

Deactivation rates for I_{Ks} were measured by depolarizing cells to 30 mV for 2 s, followed by a tail-pulse from −60 mV to −30 mV in 10-mV increments. Figure 3B shows the time constant for deactivation plotted as a function of tail-pulse potential. Compared with WT, G269S significantly accelerated the deactivation rates between −60 mV and −30 mV. In addition, coexpressing WT with increasing amounts of G269S showed a concentration-dependent acceleration of I_{Ks} deactivation kinetics.

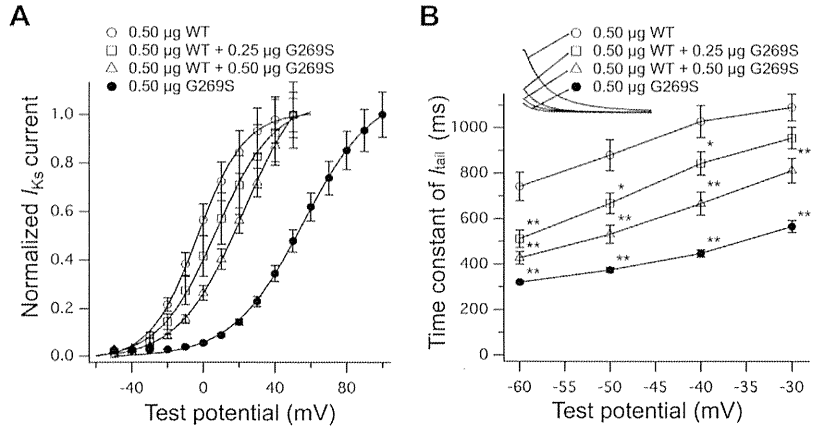

Figure 3 G269S Affects the Activation Gate of I_{Ks} Channels

(A) The normalized *I-V* relation of peak tail I_{Ks} recorded from Chinese hamster ovary cells expressing 0.5 μg *KCNE1* with 0.5 μg *KCNQ1*-WT **(open circles),** 0.5 μg *KCNQ1*-WT + 0.25 μg *KCNQ1*-G269S **(open squares),** 0.5 μg *KCNQ1*-WT + 0.5 μg *KCNQ1*-G269S **(open triangles),** and 0.5 μg *KCNQ1*-G269S **(solid circles). (B)** Deactivation time constants (τ) obtained by fitting the tail I_{Ks} decay (inset) to a single exponential function for voltages between –60 mV and –30 mV. *p < 0.05 and **p < 0.01 versus *KCNQ1*-WT. Abbreviations as in Figure 2.

Effects of G269S mutant subunits on the expression of *KCNQ1* tetramers. Figure 4 shows microscopic phase contrast (Fig. 4A) and confocal images (Fig. 4B) of 3 CHO cells expressing *KCNE1* with *KCNQ1*-WT, WT + G269S mutation, and G269S alone. *KCNQ1*-WT proteins were amply transported to the cell membrane. In cells expressing G269S alone, G269S proteins were mostly distributed in the cytosol. In cells expressing WT + G269S, WT + G269S proteins were expressed both on the cell membrane and in the cytosol, suggesting that the cell membrane expression of channel proteins is increased by the coexpression of WT subunits.

I_{Ks} reconstituted with G269S mutant reduces its responses to PKA stimulation. To explain how G269S may be causing adrenergic-induced prolongation of QTc intervals, we tested whether G269S might impair the PKA-mediated regulation of I_{Ks} in HEK293 cells expressing *KCNQ1*-WT and/or G269S with *KCNE1* and Yotiao protein (8) (we failed to record the response of I_{Ks} to beta-adrenergic agonist isoproterenol or PKA stimulation in CHO cells).

In cells expressing WT, both isoproterenol (100 nmol/l) (Fig. 5A) and a PKA-stimulating cocktail (5 μmol/l FK + 15 μmol/l IBMX) (Fig. 5B) increased tail I_{Ks} density by ~100%. In contrast, cells expressing G269S or WT + G269S dramatically reduced the response of the peak tail I_{Ks} to isoproterenol or the PKA stimulation. Figure 5C shows the bar graphs that summarize the percent increase in tail I_{Ks} densities. These data suggest that G269S blunted the response of I_{Ks} to beta-adrenergic agonist or PKA stimulation.

Table 1 *KCNQ1*-G269S Affects the Activation Gate of I_{Ks} Channels

	n	V_h (mV)	*k* (mV)
0.50 μg WT	15	−2.4 ± 1.7	13.2 ± 0.4
0.50 μg WT + 0.25 μg G269S	13	8.9 ± 3.3*	15.2 ± 0.4*
0.50 μg WT + 0.50 μg G269S	11	25.4 ± 5.2*	17.8 ± 0.8*
0.50 μg G269S	13	68.3 ± 8.3*	23.4 ± 1.8*

Values are mean ± SD. *p < 0.01 versus WT.
I_{Ks} = slow component of delayed rectifier K^+ current; WT = wild type.

G269S prevents the increase in I_{Ks} caused by the phosphomimetic S27D mutation. To elucidate further the mechanism underlying the attenuation of this PKA-mediated phosphorylation by G269S mutation, we engineered the phosphomimetic *KCNQ1*-S27D mutation with or without G269S mutation (14) and examined I_{Ks} recapitulated by coexpressing *KCNE1* and Yotiao (Fig. 6).

Compared with WT, S27D increased I_{Ks} amplitudes considerably (Figs. 6A and 6B), which is similar to what was reported previously (14,15). Figure 6C shows that, consistent with S27D mimicking a PKA phosphorylated I_{Ks} channel, the application of 100 nmol/l of isoproterenol only slightly affected the peak tail I_{Ks} (14.1 ± 5.5%, n = 7). In contrast, compared with G269S, S27D-G269S did not increase peak tail I_{Ks} (Figs. 6D and 6E). The data are summarized in Figure 6F. Therefore, G269S prevents PKA up-regulation of I_{Ks} even if S27 is phosphorylated.

Discussion

The present study revealed that G269S causes adrenergic-induced LQT, exerts a moderate dominant-negative suppression on the I_{Ks} channel, and prevents up-regulation in response to PKA stimulation. The exercise-dependent unmasking of QTc prolongation observed in our G269S

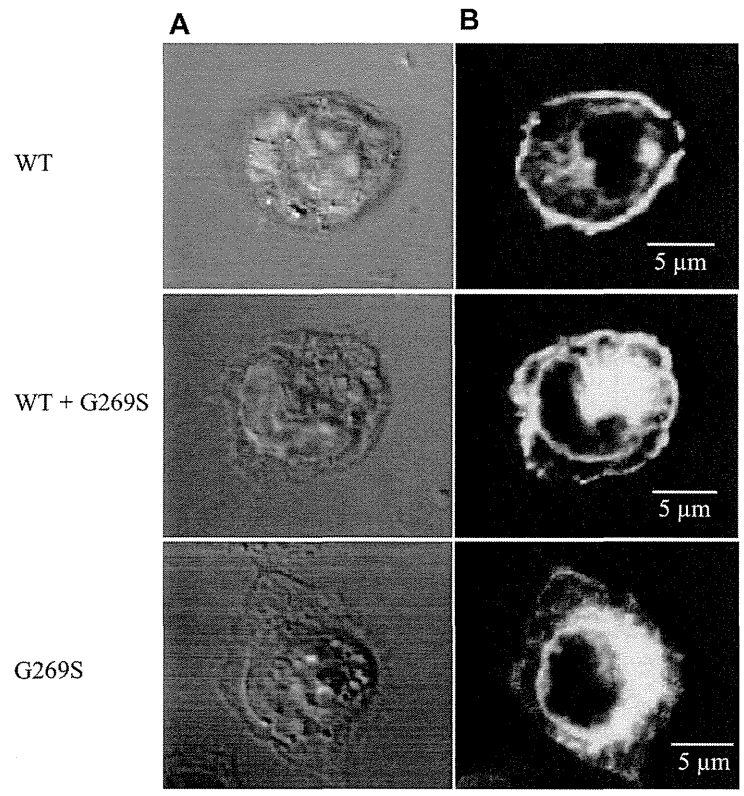

Figure 4 **Cellular Localization of *KCNQ1* Proteins in CHO Cells**

Microscopic phase contrast images **(A)** and corresponding confocal images **(B)** are shown of representative Chinese hamster ovary (CHO) cells coexpressing 0.5 μg *KCNE1* and 0.5 μg *KCNQ1*-WT **(upper)**, 0.5 μg *KCNQ1*-WT + 0.5 μg *KCNQ1*-G269S **(middle)**, or 0.5 μg *KCNQ1*-G269S **(lower)**. The cells were immunostained with an anti-*KCNQ1* antibody. WT = wild type.

patients is likely due to an adrenergic up-regulation of $I_{Ca,L}$ without concomitant up-regulation of I_{Ks}.

Approximately 20% to 25% of genotype-confirmed LQTS patients have a normal range of QTc (16,17) and the percentage of these silent mutation carriers is significantly higher in LQT1 (36%) than in the other 2 major types of LQTS (LQT2, 19%, and LQT3, 10%). Lethal arrhythmias can occur in these apparently healthy silent mutation carriers without any premonitory sign (4,18). Several cases of physical-exertion–triggered cardiac events (including death) have been reported in silent G269S carriers (10–12).

Mutations in *KCNQ1* are responsible for defects in I_{Ks}, which is the main outward component in maintaining cardiac repolarization reserve and highly sensitive to catecholamines (5,19). Functional analysis showed that G269S mutation reduced I_{Ks} density independent of changes in gating, shifted the *I-V* relation to a more depolarizing direction, and accelerated the deactivation time course. Taken together, G269S mutation exerted "loss-of-function" effects on the I_{Ks} channel.

Immunocytochemical studies (Fig. 4) indicated that G269S decreased cell surface expression of channel proteins. However, the trafficking-deficiency was partially rescued by coexpression of the WT subunits, resulting in the increased expression of channel proteins on the cell membrane. In contrast to the trafficking-deficient LQT1 mutations *KCNQ1*-ΔS276 and T587M (7,20), G269S appeared to form heteromultimers with WT and traffic to the cell membrane. We suspect that the partial correction of the G269S trafficking-deficient phenotype by coexpression with WT might partially explain why the clinical phenotype of *KCNQ1*-G269S mutation carriers is mild despite the observation that the channels are functionally defective.

In human ventricular myocytes, the rapid component of delayed rectifier K^+ current, I_{Kr}, and $I_{Ca,L}$ normally play the dominant role in regulating the ventricular action potential at rest (21,22). Therefore, *KCNQ1* mutations (e.g., G269S) that cause a mild-to-moderate functional defect in I_{Ks} might ordinarily have little effect on the ventricular action potential. In contrast, I_{Ks} plays a major role in regulating the ventricular action potential after adrenergic stimulation,

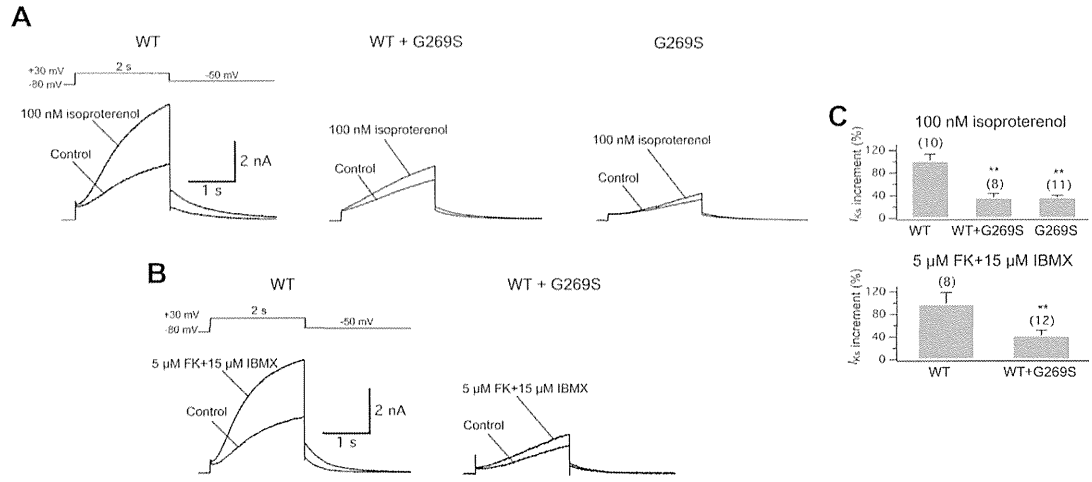

Figure 5 I_{Ks} **Reconstituted With *KCNQ1*-G269S Reduced Responses to PKA Stimulation**

Superimposition of I_{Ks} traces recorded from human embryonic kidney 293 cells expressing 2 μg Yotiao + 0.5 μg *KCNE1* with 0.5 μg *KCNQ1*-WT, 0.5 μg *KCNQ1*-WT + 0.5 μg *KCNQ1*-G269S, and 0.5 μg *KCNQ1*-G269S before and after bath application of 100 nmol/l isoproterenol **(A)** or 5 μmol/l forskolin (FK) + 15 μmol/l 3-isobutyl-l-methyl-xanthine (IBMX) **(B)**. **(C)** The percentage increase in tail I_{Ks} after bath application of 100 nmol/l isoproterenol **(upper)** and 5 μmol/l FK + 15 μmol/l IBMX **(lower)**. **p < 0.01 versus *KCNQ1*-WT. PKA = protein kinase A; other abbreviations as in Figure 2.

which activates I_{Ks} to prevent excessive ventricular action potential duration or QT prolongation by $I_{Ca,L}$ (8,23). The role that I_{Ks} plays during adrenergic stimulation may explain why 62% of cardiac events in LQT1 patients occur during exercise (8,9). The blunted response of G269S channels to both beta-adrenergic agonist and PKA stimulation (Fig. 5) may result in excessive ventricular action potential duration and QTc prolongation specifically during exercise.

Consistent with previous reports (14,15), our experiments also demonstrated that the S27D mutant mimicked the PKA-mediated phosphorylation of I_{Ks} channels and increased I_{Ks} (Fig. 6). In contrast, S27D did not mimic

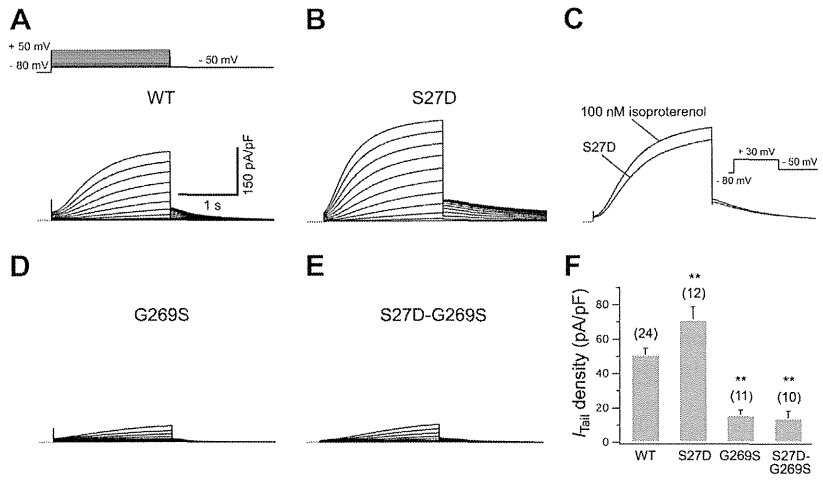

Figure 6 **G269S Prevents the Increase in I_{Ks} Caused by the Phosphomimetic S27D Mutation**

Representative current traces recorded from human embryonic kidney 293 cells expressing 2 μg Yotiao + 0.5 μg *KCNE1* with 0.5 μg *KCNQ1*-WT **(A)**, 0.5 μg S27D **(B)** and exposure to 100 nmol/l isoproterenol **(C)**, 0.5 μg G269S **(D)**, and 0.5 μg S27D-G269S **(E)**, respectively. I_{Ks} was elicited by the same protocol as that in Figure 2A (inset). **(F)** Bar graphs show effects of G269S on tail I_{Ks} densities recorded on repolarization to –50 mV following a 2-s depolarization to 30 mV for the different transfection conditions. **p < 0.01 versus *KCNQ1*-WT. Abbreviations as in Figure 2.

PKA phosphorylation of I_{Ks} with G269S mutation. Therefore, G269S appears to prevent the functional effect that phosphorylation at S27 has on I_{Ks}.

Several groups have recently reported that different LQT1 mutations reduce the PKA sensitivity of I_{Ks}. Heijman et al. (15) reported that the A341V, which predisposes patients to a severe form of LQT1 (24), is also less sensitive to PKA stimulation. The decreased sensitivity to PKA is because A341V blunts phosphorylation at S27. Consistent with this, compared with cells expressing A341V, cells expressing S27D-A341V mimicked PKA stimulation and caused an up-regulation in I_{Ks}. We show a novel mechanism for PKA insensitivity. Unlike S27D-A341V, S27D-G269S did not mimic PKA stimulation of I_{Ks}, suggesting that G269S dissociates the link between phosphorylation at S27 and up-regulation of I_{Ks}.

Additionally, Barsheshet et al. (25) showed that patients with LQT1 mutations in the cytoplasmic loops between the S2 and S3 or S4 and S5 have a high risk for life-threatening events and derive a benefit from treatment with beta-adrenergic blockers. These mutations generate I_{Ks}, which is also resistant to PKA activation. Our findings first demonstrated that a "latent" LQT1 mutation could also be insensitive to PKA stimulation, which may explain the unmasking of the latent LQT1 phenotype that occurs during exercise. Consistent with the previous findings (25), the cardiac events of our symptomatic G269S patient have disappeared since beginning beta-blocker therapy for 42 months. This suggests that beta-adrenergic therapy would also be effective in patients with latent LQT1 mutations such as G269S. We speculate that beta-blocker therapy is effective because it would inhibit adrenergic-induced increases in $I_{Ca,L}$, which would minimize QTc prolongation with exercise.

Study limitations. In the present study, we screened the mutations that are responsible for LQT1, 2, 3, 5, 6, and 7. Therefore, the comorbidity of other types of LQTS was not completely excluded, although their frequency was quite low. In addition, only one patient was symptomatic of cardiac event and received beta-adrenergic blocker. Further studies are required to confirm that beta-blocker therapy may protect individuals who carry KCNQ1 mutations insensitive to PKA regulation.

Conclusions

We found that G269S caused moderate functional dysfunction in control conditions but almost completely disrupted PKA mediated up-regulation in I_{Ks}. This is likely why the G269S patients have borderline resting QTc intervals but significantly longer QTc while exercising.

Acknowledgments

The authors thank Dr. Daniel C. Bartos (Department of Physiology, University of Kentucky, Kentucky) for the *KCNQ1*-S27D mutation; Dr. J. Barhanin (Institut de Pharmacologie Moleculaire et Cellulaire, CNRS, Valbonne, France) for the gift of *KCNQ1*-WT; and Dr. J Kurokawa (Department of Bio-Informational Pharmacology, Tokyo Medical and Dental University, Japan) for the full-length cDNA encoding human A-kinase-anchoring protein 9 subcloned into pCDNA3.1 expression vector.

Reprint requests and correspondence: Dr. Minoru Horie, Department of Cardiovascular and Respiratory Medicine, Shiga University of Medical Science, Seta-Tsukinowa-cho, Otsu, Shiga 520-2192, Japan. E-mail: horie@belle.shiga-med.ac.jp.

REFERENCES

1. Roden DM. Clinical practice: long-QT syndrome. N Engl J Med 2008;358:169–76.
2. Schwartz PJ, Crotti L, Insolia R. Long-QT syndrome: from genetics to management. Circ Arrhythm Electrophysiol 2012;5:868–77.
3. Napolitano C, Priori SG, Schwartz PJ, et al. Genetic testing in the long QT syndrome: development and validation of an efficient approach to genotyping in clinical practice. JAMA 2005;294:2975–80.
4. Shimizu W, Horie M. Phenotypic manifestations of mutations in genes encoding subunits of cardiac potassium channels. Circ Res 2011;109: 97–109.
5. Sanguinetti MC, Curran ME, Zou A, et al. Coassembly of K(V)LQT1 and minK (IsK) proteins to form cardiac I(Ks) potassium channel. Nature 1996;384:80–3.
6. Moss AJ, Shimizu W, Wilde AA, et al. Clinical aspects of type-1 long-QT syndrome by location, coding type, and biophysical function of mutations involving the KCNQ1 gene. Circulation 2007;115: 2481–9.
7. Gouas L, Bellocq C, Berthet M, et al., for the D.E.S.I.R. Study Group. New KCNQ1 mutations leading to haploinsufficiency in a general population: defective trafficking of a KvLQT1 mutant. Cardiovasc Res 2004;63:60–8.
8. Marx SO, Kurokawa J, Reiken S, et al. Requirement of a macromolecular signaling complex for beta adrenergic receptor modulation of the *KCNQ1-KCNE1* potassium channel. Science 2002;295:496–9.
9. Schwartz PJ, Priori SG, Spazzolini C, et al. Genotype-phenotype correlation in the long-QT syndrome: gene-specific triggers for life-threatening arrhythmias. Circulation 2001;103:89–95.
10. Chen S, Zhang L, Bryant RM, et al. KCNQ1 mutations in patients with a family history of lethal cardiac arrhythmias and sudden death. Clin Genet 2003;63:273–82.
11. Ackerman MJ, Tester DJ, Porter CJ. Swimming, a gene-specific arrhythmogenic trigger for inherited long QT syndrome. Mayo Clin Proc 1999;74:1088–94.
12. Creighton W, Virmani R, Kutys R, Burke A. Identification of novel missense mutations of cardiac ryanodine receptor gene in exercise-induced sudden death at autopsy. J Mol Diagn 2006;8:62–7.
13. Takenaka K, Ai T, Shimizu W, et al. Exercise stress test amplifies genotype-phenotype correlation in the LQT1 and LQT2 forms of the long-QT syndrome. Circulation 2003;107:838–44.
14. Kurokawa J, Chen L, Kass RS. Requirement of subunit expression for cAMP-mediated regulation of a heart potassium channel. Proc Natl Acad Sci USA 2003;100:2122–7.
15. Heijman J, Spätjens RL, Seyen SR, et al. Dominant-negative control of cAMP-dependent I_{Ks} upregulation in human long-QT syndrome type 1. Circ Res 2012;110:211–9.
16. Priori SG, Schwartz PJ, Napolitano C, et al. Risk stratification in the long-QT syndrome. N Engl J Med 2003;348:1866–74.
17. Goldenberg I, Horr S, Moss AJ, et al. Risk for life-threatening cardiac events in patients with genotype-confirmed long-QT syndrome and normal-range corrected QT intervals. J Am Coll Cardiol 2011;57:51–9.
18. Schwartz PJ. The long QT syndrome. In: Kulbertus HE, Wellens HJJ, editors. Sudden Death. The Hague, the Netherlands: Martinus Nijhoff, 1980:358–78.
19. Sanguinetti MC. Long QT syndrome: ionic basis and arrhythmia mechanism in long QT syndrome type 1. J Cardiovasc Electrophysiol 2000;11:710–2.

20. Yamashita F, Horie M, Kubota T, et al. Characterization and subcellular localization of KCNQ1 with a heterozygous mutation in the C-terminus. J Mol Cell Cardiol 2001;33:197–207.
21. Jost N, Virág L, Bitay M, et al. Restricting excessive cardiac action potential and QT prolongation: a vital role for I_{Ks} in human ventricular muscle. Circulation 2005;112:1392–9.
22. O'Hara T, Virág L, Varro A, Rudy Y. Simulation of the undiseased human cardiac ventricular action potential: model formulation and experimental validation. PLoS Comput Biol 2011;7:1–29.
23. McDonald TF, Pelzer S, Trautwein W, Pelzer DJ. Regulation and modulation of calcium channels in cardiac, skeletal, and smooth muscle cells. Physiol Rev 1994;74:365–507.
24. Crotti L, Spazzolini C, Schwartz PJ, et al. The common long-QT syndrome mutation KCNQ1/A341V causes unusually severe clinical manifestations in patients with different ethnic backgrounds: toward a mutation-specific risk stratification. Circulation 2007;116:2366–75.
25. Barsheshet A, Goldenberg I, O-Uchi J, et al. Mutations in cytoplasmic loops of the KCNQ1 channel and the risk of life-threatening events: implications for mutation-specific response to beta-blocker therapy in type-1 long QT syndrome. Circulation 2012;125:1988–96.

Key Words: heterologous expression ▪ *KCNQ1* mutation ▪ long QT syndrome ▪ protein kinase A stimulation.

Original Article

A Mutation Causing Brugada Syndrome Identifies a Mechanism for Altered Autonomic and Oxidant Regulation of Cardiac Sodium Currents

Takeshi Aiba, MD, PhD*; Federica Farinelli, PhD*; Geran Kostecki, BS; Geoffrey G. Hesketh, PhD; David Edwards, MD, PhD; Subrata Biswas, PhD; Leslie Tung, PhD; Gordon F. Tomaselli, MD

Background—The mechanisms of the electrocardiographic changes and arrhythmias in Brugada syndrome (BrS) remain controversial. Mutations in the sodium channel gene, *SCN5A*, and regulatory proteins that reduce or eliminate sodium current (I_{Na}) have been linked to BrS. We studied the properties of a BrS-associated *SCN5A* mutation in a protein kinase A (PKA) consensus phosphorylation site, R526H.

Methods and Results—In vitro PKA phosphorylation was detected in the I-II linker peptide of wild-type (WT) channels but not R526H or S528A (phosphorylation site) mutants. Cell surface expression of R526H and S528A channels was reduced compared with WT. Whole-cell I_{Na} through all channel variants revealed no significant differences in the steady-state activation, inactivation, and recovery from inactivation. Peak current densities of the mutants were significantly reduced compared with WT. Infection of 2D cultures of neonatal rat ventricular myocytes with WT and mutant channels increased conduction velocity compared with noninfected cells. PKA stimulation significantly increased peak I_{Na} and conduction velocity of WT but not mutant channels. Oxidant stress inhibits cardiac I_{Na}; WT and mutant I_{Na} decreases with the intracellular application of reduced nicotinamide adenine dinucleotide (NADH), an effect that is reversed by PKA stimulation in WT but not in R526H or S528A channels.

Conclusions—We identified a family with BrS and an *SCN5A* mutation in a PKA consensus phosphorylation site. The BrS mutation R526H is associated with a reduction in the basal level of I_{Na} and a failure of PKA stimulation to augment the current that may contribute to the predisposition to arrhythmias in patients with BrS, independent of the precipitants. ***(Circ Cardiovasc Genet.* 2014;7:249-256.)**

Key Words: death, sudden, cardiac ■ ion channel ■ mutation ■ reactive oxygen species

Mutations in the cardiac sodium channel gene, *SCN5A*, encoding $Na_v1.5$ currents can produce of number of heritable diseases of cardiac rhythm and contractile function. Loss-of-function mutations have been associated with sudden cardiac death and ST segment abnormalities in the right precordial leads of the ECG referred to as Brugada syndrome (BrS).[1] This may be part of a constellation of functional and structural abnormalities of the heart associated with perturbations of the ST segment.[2-4]

Clinical Perspective on p 256

BrS is characterized by ECG alterations in the right precordial leads in the absence of structural cardiac abnormalities, preponderance in men particularly of Asian descent, and a high rate of sudden cardiac death. The prevalence of type 1 ECG changes is estimated to be ≈5 of 10,000[5,6] and more than double that in Japan and other parts of Asia.[7,8] The updated expert consensus statement on heritable arrhythmias recommends that a diagnosis of BrS be made in the presence of a spontaneous or drug-induced type 1 ECG pattern in ≥1 right precordial lead (V_1 through V_3).[9]

The genetic mechanisms of BrS have provided insights into the links between metabolism, ion channel function, and cardiac arrhythmias. Approximately 20% of BrS is associated with mutations in *SCN5A*.[10,11] In *SCN5A*-linked BrS, there is a reduction in Na current (I_{Na}) density that may result from mutations in the channel subunits or in modifiers of Na channel function. Mutations in glycerol phosphate dehydrogenase 1-like (*GPD1-L*), which is >80% homologous with glycerol phosphate dehydrogenase 1 (*GPD1*),[12] reduce I_{Na} through

Received August 26, 2013; accepted March 23, 2014.

From the Division of Cardiology, Department of Internal Medicine, Johns Hopkins University School of Medicine, Baltimore, MD (T.A., F.F., D.E., S.B., G.F.T.); and Department of Biomedical Engineering (G.K., L.T.) and Department of Biological Chemistry (G.G.H.), Johns Hopkins University, Baltimore, MD.

The current address for Dr Aiba is Division of Arrhythmia and Electrophysiology, National Cerebral and Cardiovascular Center, Suita, Osaka, Japan.

*Drs Aiba and Farinelli contributed equally to this work.

The Data Supplement is available at http://circgenetics.ahajournals.org/lookup/suppl/doi:10.1161/CIRCGENETICS.113.000480/-/DC1.

Correspondence to Gordon F. Tomaselli, MD, Division of Cardiology, Department of Internal Medicine, Johns Hopkins University School of Medicine, 720 N Rutland Ave, Ross 844, Johns Hopkins University, Baltimore, MD 21205. E-mail gtomasel@jhmi.edu

© 2014 American Heart Association, Inc.

Circ Cardiovasc Genet **is available at http://circgenetics.ahajournals.org** **DOI: 10.1161/CIRCGENETICS.113.000480**

Downloaded from http://circgenetics.ahajournals.org at National Cardiovascular Center on June 18, 2014

nicotinamide adenine dinucleotide/reduced nicotinamide adenine dinucleotide (NADH)-dependent mechanisms[13,14] via activation of protein kinase C (PKC).[15] There is evidence to support a direct effect on $Na_V1.5$ by PKC phosphorylation[15] and an NADH/PKC-mediated overproduction of reactive oxygen species (ROS) leading to a reduction in expressed I_{Na}.[14] These data suggest that inhibition of I_{Na} by pyridine nucleotides is mediated by mitochondrial-produced ROS and that protein kinase A (PKA) activation may block ROS-induced reduction of the current and constitutes a treatment strategy for patients with BrS.[13,16]

We studied a mutation in a patient with BrS presenting with a spontaneous type 1 ECG and history of syncope to elucidate the mechanism(s) of I_{Na} reduction and its reversal by adrenergic activation. Our data suggest a mechanism for the ECG changes and arrhythmias in BrS initiated by altered metabolism and an increase in oxidant burden that is not mitigated by β-adrenergic stimulation.

Materials and Methods

Detailed methods are provided in the Data Supplement. Molecular biological reagents including lentiviral vectors[17–19] and ion channel plasmids were generated as previously described.[20] All protocols followed US Department of Agriculture and National Institutes of Health guidelines and were approved by the Animal Care and Use Committee of the Johns Hopkins Medical Institutions.

Neonatal rat ventricular myocytes (NRVMs) were enzymatically isolated[21] and transduced as previously described.[18,22] Optical mapping was performed on plated monolayers of NRVMs, and data were analyzed using custom-written scripts in MATLAB (Mathworks, Natick, MA).[22]

Whole-cell I_{Na} was measured under voltage clamp at room temperature (22°C) as previously described.[23] The bath and pipette solutions are described in the Data Supplement. Recombinant human $Na_V1.5$ peptides were expressed in *Escherichia coli*, purified, and incubated with PKA in the presence of γP^{32}-labeled ATP. HEK 293 cells were transformed with wild-type (WT) $Na_V1.5$, R526H, and S528A $Na_V1.5$ plasmids. Cell membrane proteins were labeled with biotin and captured on streptavidin beads. Total and membrane-bound $Na_V1.5$ expression was determined by Western blotting using an anti-Na channel antibody (Sigma S8809).

The results are presented as mean±SD or SEM. Statistical comparisons were made using a 1-way ANOVA followed by Bonferroni/Dunn tests for multiple comparisons, and serial studies were assessed by repeated-measures ANOVA. Statistical significance was assumed at $P<0.05$.

Results

The patient is a 33-year-old man who presented with 2 syncopal spells in rapid succession during micturition and without premonitory symptoms. In the field, he had a normal heart rate and blood pressure. He had experienced palpitations after vigorous exercise in the past but had never had syncope. There was a family history of a paternal aunt who died suddenly around age 40 of unknown causes and a maternal uncle with Down Syndrome who died suddenly at age 11 in the setting of a febrile illness. The mutation was transmitted maternally, and the proband's mother had multiple episodes of syncope and near syncope associated with migraine headaches which were felt to be vasodepressor. Her baseline ECG exhibited 0.5- to 1-mm J-point elevation in leads V_1 and V_2 and a saddleback segment in V_2; after procainamide infusion, both V_1 and V_2 ST segments were changed into a coved type (Figure SI in the Data Supplement). The patient's younger sister carries the mutation and has a baseline incomplete right bundle-branch block (RBBB), which did not change with procainamide infusion.

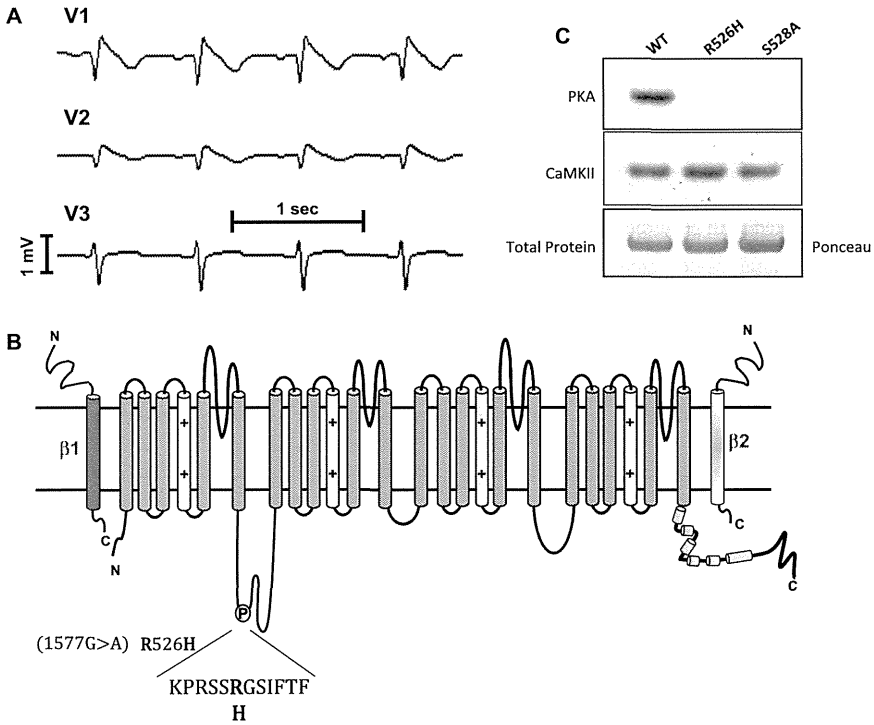

Figure 1. A, Leads V_1 through V_3 of the patient's ECG exhibit typical domed J-point elevation. **B**, A schematic of the $Na_V1.5$ pore-forming α-subunit and the β1 and β2 subunits. The disease-causing mutation (R526H) is in the I-II interdomain linker of $Na_V1.5$ in a canonical protein kinase A (PKA) phosphorylation recognition sequence. The residue 2 amino acids C-terminal to R526, S528 was mutated to alanine in this study. **C**, In vitro phosphorylation of I-II linker peptides. Purified fragments were incubated with PKA and calcium-calmodulin kinase II δ (CaMKII) in the presence of γP^{32}-labeled ATP. The labeled peptides were separated by polyacrylamide gel electrophoresis (PAGE). Mutant peptides R526H and S528A are not labeled by PKA but are phosphorylated as efficiently as wild type (WT) in the presence of CaMKII.

Downloaded from http://circgenetics.ahajournals.org/ at National Cardiovascular Center on June 18, 2014

His 12-lead ECG revealed coved ST segments in leads V_1 and V_2 consistent with a Brugada type 1 ECG pattern (Figure 1A). A transthoracic echocardiogram was normal. A single-chamber defibrillator was implanted.

BrS Mutation Disables PKA Phosphorylation

DNA sequencing of *SCN5A* revealed a nucleotide transition at position 1577 encoding a missense mutation at codon 526 changing an arginine to histidine (R526H, Figure 1B). The minor allele frequency from the exome variant server is 0.016%[24] and is a chemically and structurally conservative change.[25,26] However, the mutation resides in a PKA recognition sequence in the I-II interdomain linker of the channel, with serine 528 (S528) as the phosphorylated residue.

The I-II linker of $Na_V1.5$ contains consensus phosphorylation sites for several kinases including PKA and calcium calmodulin kinase II. We created mutant I-II linker peptides with the clinical mutation, R526H, and at the putative phosphorylation site, S528A. In vitro phosphorylation by PKA revealed complete elimination of ^{32}P incorporation into the R526H and S528A peptides. By contrast, calcium calmodulin kinase II phosphorylated all channel peptides equally (Figure 1C).

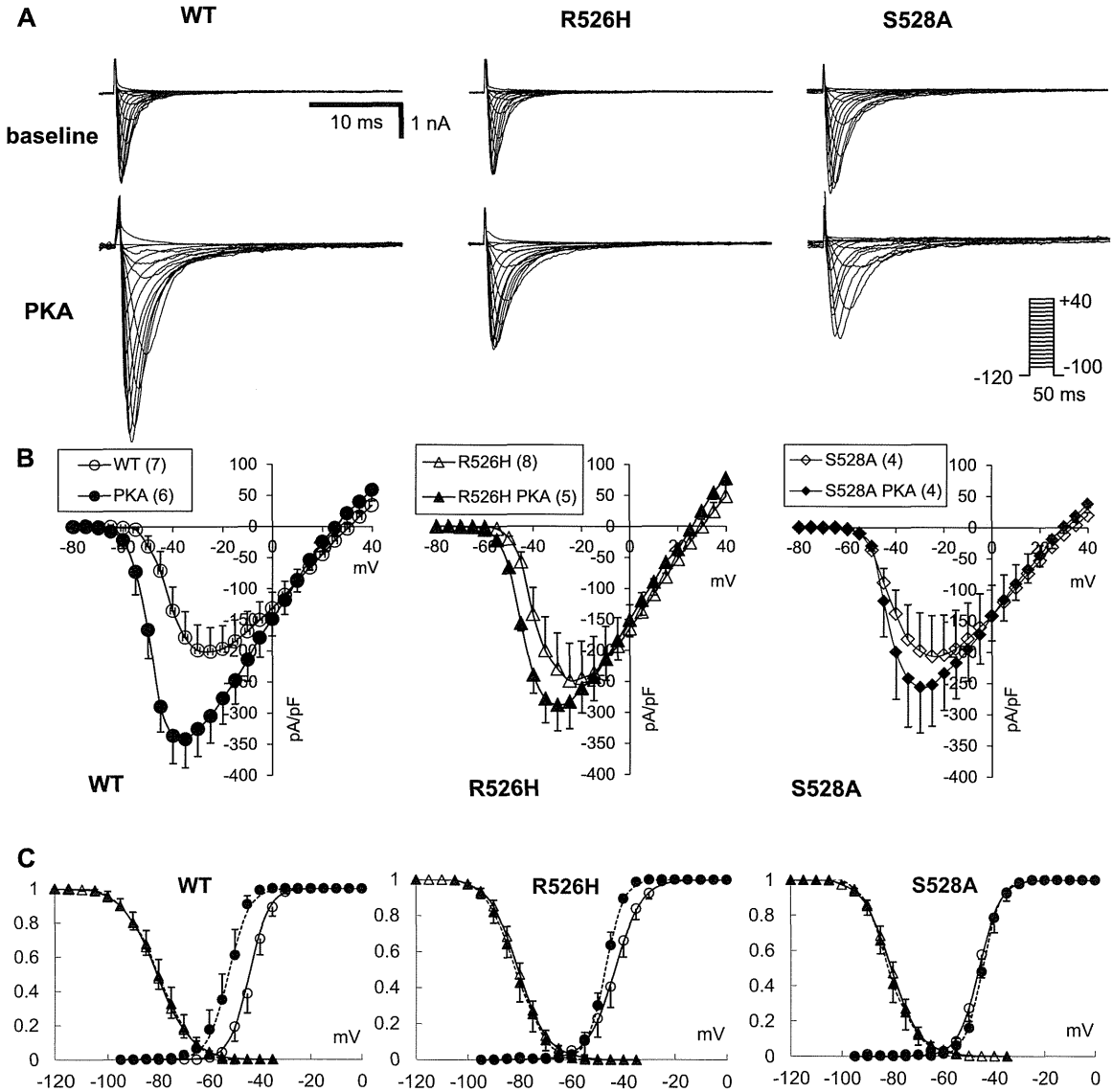

Figure 2. Protein kinase A (PKA) regulation of Na current variants. **A**, Representative families of current through wild-type (WT), R526H, and S528A channels expressed in HEK 293 cells in the presence and absence of PKA activation. **B**, I–V relationships in the presence (filled symbols) and absence (open symbols) of PKA stimulation. There is no increase in the current through the mutant channels. **C**, Activation (circles) and steady-state inactivation (triangles) curves in the presence (filled symbols) and absence (open symbols) of PKA stimulation. The data are fit to a Boltzman function as described in the Materials and Methods section. There are no significant differences between the WT and mutant channels in the basal voltage dependence and kinetics of gating.

Downloaded from http://circgenetics.ahajournals.org/ at National Cardiovascular Center on June 18, 2014

Altered Channel Regulation in Response to Stress

We speculate that stressors that reduce I_{Na} density (oxidants, fever, and Na channel blocking drugs) may, in part, be offset by PKA stimulation of the channel. To study the functional effects of these mutations in response to PKA phosphorylation, we expressed WT and mutant $Na_V1.5$ currents in HEK 293 cells. Selected families of currents in standard recording solutions revealed current densities through the mutant channels that were only modestly smaller than WT but not different from each other in the absence of PKA stimulation (Figure 2A and 2B). The baseline whole-cell properties including the current–voltage (I–V) relationships, voltage dependence and kinetics of gating, and kinetics of current decay were not different between WT and the mutants (Figure 2C; Table SI in the Data Supplement). In the presence of PKA, WT $Na_V1.5$ currents were significantly upregulated with a hyperpolarizing shift in the peak I–V and activation curves (Figure 2) and hastened recovery from inactivation (Table SI in the Data Supplement). By contrast, neither the peak current, voltage dependence of gating, or recovery kinetics (Figure 2; Table SI in the Data Supplement) of R526H or S528A were significantly affected by the addition of PKA.

Oxidative stress and an increase in glycolysis will lead to increased levels of cytosolic NADH, which rapidly decreases I_{Na}. We recorded currents in a metabolic stabilizing solution (see Methods in Data Supplement, inhibiting kinases and phosphatases) to examine the effect of intracellular NADH on the WT and mutant currents. The baseline peak density of the WT current was significantly larger than either R526H or S528A mutant currents (Figure 3A–3C). The addition of 100 μmol/L NADH to the pipette solution reduced the average I_{Na} by >50% in all channel variants (Figure 3A and 3B). The addition of NADH had no significant effect on the decay kinetics or voltage dependence of gating of WT $Na_V1.5$ or the mutant channels (Figure 3E; Table SII in the Data Supplement). We speculated that the current density might be restored by PKA in the setting of an increase in NADH and that this restoration might be compromised in the mutant channels. To study the effect of activation of PKA signaling on NADH-induced suppression of $Na_V1.5$ current, cells were incubated with forskolin and 8-Br cAMP for 20 minutes

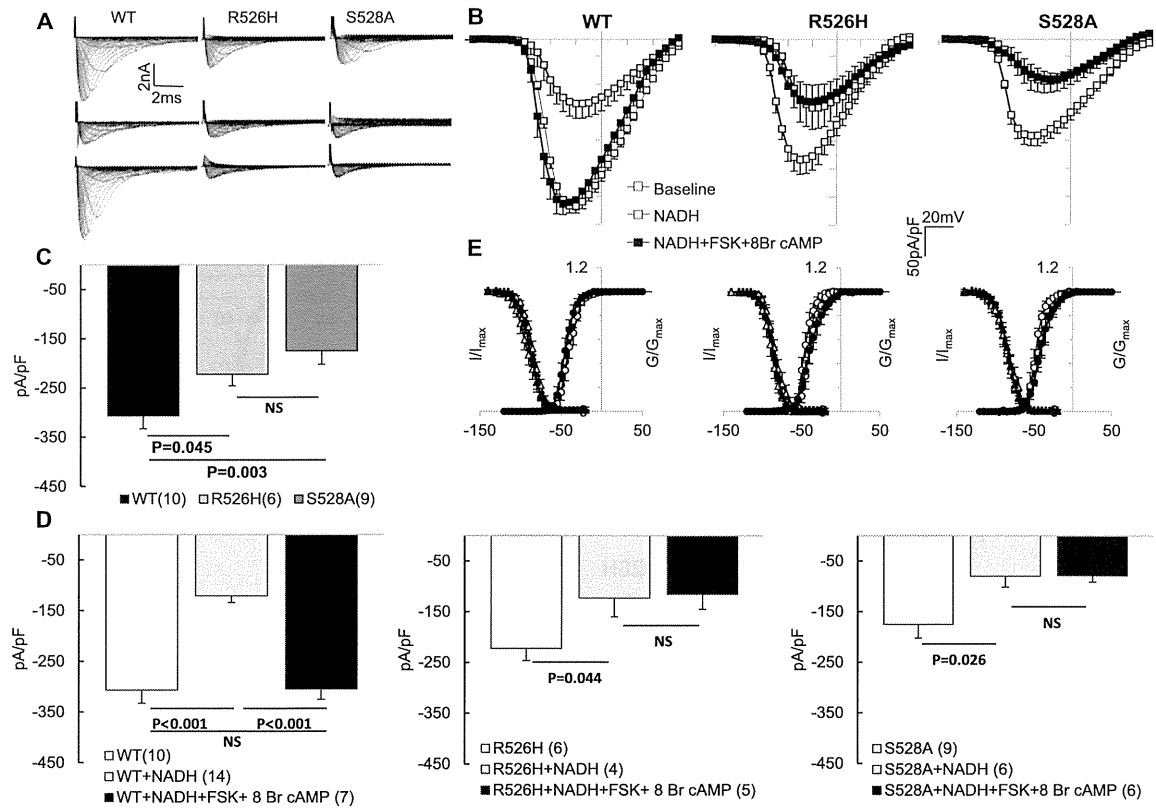

Figure 3. Regulation of Na channel variants by reduced nicotinamide adenine dinucleotide (NADH) and protein kinase A (PKA). The currents are recorded with fluoride in the pipette. **A**, Representative families of current through wild-type (WT), R526H, and S528A channels expressed in HEK 293 cells (**top**) in the presence of 100 μmol/L NADH (**middle**) and NADH plus PKA activation with forskolin (FSK) and 8-Br-cAMP (**bottom**). **B**, I–V relationships in the absence (open squares) and presence of NADH (gray squares) and NADH+PKA stimulation (filled squares). NADH reduces the current through all channel variants, whereas PKA activation does not increase the current density through the mutant channels. **C**, Bar plots of peak current densities of WT (black), R526H (blue), and S528A (red) under basal conditions. **D**, Summary bar plots for WT, R526H, and S528A channel peak current density at baseline (open bars) with NADH (gray bars) and NADH+PKA activation (black bars). **E**, Activation and steady-state inactivation curves in the absence (open circles activation, open triangles inactivation) and presence of NADH (gray circles activation, gray triangles inactivation) and NADH + PKA stimulation (filled circles activation, filled triangles inactivation) for each of the channel variants; there are no significant differences in any of the variants under any of the conditions.

Downloaded from http://circgenetics.ahajournals.org/ at National Cardiovascular Center on June 18, 2014

prior to patch clamp recording. Incubation with forskolin and 8-Br cAMP completely reversed the downregulation of WT $Na_v1.5$ current by intracellular NADH (Figure 3A, 3B, and 3D) and produced a modest but significant hyperpolarizing shift in the voltage dependence of activation gating (Table SII in the Data Supplement). The reductions in R526H and S528A currents by NADH were not affected by the addition of forskolin and 8-Br cAMP (Figure 3D; Table SII in the Data Supplement).

Trafficking of Mutant Channels

The reduction in basal current density of R526H and S528A channels without a change in biophysical characteristics compared with WT suggested the possibility of an alteration in trafficking to the surface membrane. Surface membrane expression of WT and mutant $Na_v1.5$ channels in HEK 293 was quantified by labeling intact cells with biotin and purifying the protein on immobilized streptavadin. Overall expression of the channel proteins did not differ; however, Figure 4A illustrates that even with less WT $Na_v1.5$ protein in the total lysate, a greater proportion of the WT channel was biotinylated compared with both the R526H and S528A mutants (Figure 4B).

To study trafficking in a cardiac cell background, NRVMs were infected with lentiviruses containing the WT or mutant channels fused to enhanced green fluorescent protein (eGFP) at the carboxyl terminus. The channel-infected NRVMs were cotransfected with an endoplasmic reticulum marker dsRED-ER. Consistent with the biotinylation experiments, NRVMs infected with the viruses encoding the R526H and S528A mutants exhibited more channel protein in subcellular membranes, colocalized with dsRED-ER compared with WT channels (Figure 4C and 4D).

Effect of Mutants on Conduction Velocity

The functional consequences of the reduced surface expression and altered regulation of the mutant channels were studied using optical mapping of 2D cultures of NRVMs. To control for variability in baseline conduction velocities (CVs), cultures that were transduced with Na channel variants were compared with naïve nontransfected cultures. The cultures were stimulated over a range of pacing cycle lengths (175–500 ms) to determine the CVs; isochronal maps at baseline and in the presence of isoproterenol are shown for WT, R526H, and S528A transfected cultures (Figure 5A). The baseline CVs of NRVM cultures infected with WT $Na_v1.5$ and the mutant channels were similar and ≈20% to 50% (5–10 cm/s) faster than nontransfected cultures over a range of pacing cycle lengths (Figure 5B).

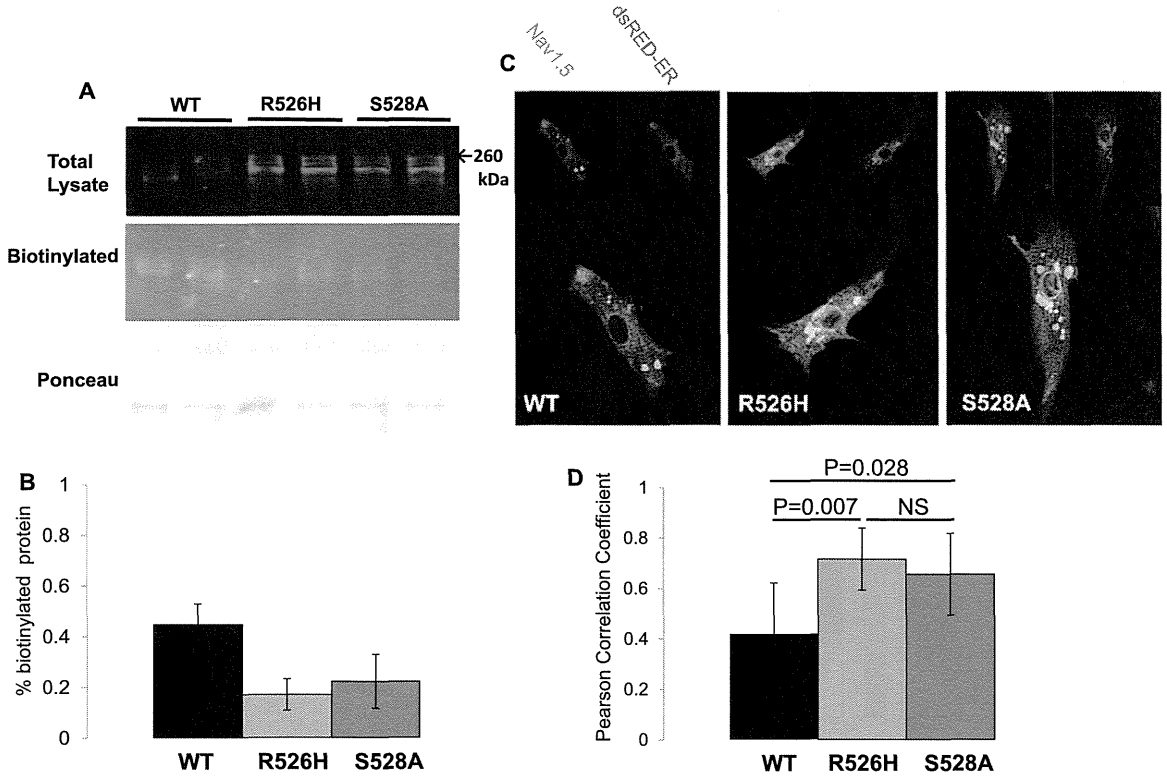

Figure 4. Mutations and channel trafficking. **A**, Surface membrane expression of the channel measured by biotinylation in intact cells. The **top** panel shows total lysate, the **middle** panel the protein captured on streptavadin beads stained with an anti-$Na_v1.5$ antibody, and the **bottom** panel is a Ponceau-stained blot demonstrating equivalent loading. **B**, The percentage of total lysate modified by biotin is significantly decreased in R526H (blue bar) and S528A (red bar) mutant channels compared with wild type (WT; black bar). **C**, Immunocytochemical localization of the channel proteins in transduced neonatal rat ventricular myocytes. The $Na_v1.5$ channel variant is cotransfected with the endoplasmic reticulum (ER) marker dsRed-ER. There is significantly increased colocalization of both mutant channel proteins with the ER marker compared with the wild type. **D**, Bar plots of the percent colocalization of the channel protein and dsRed-ER.

Downloaded from http://circgenetics.ahajournals.org/ at National Cardiovascular Center on June 18, 2014